OXIDATION AND VOLATILIZATION OF SILICA-FORMERS IN WATER VAPOR

Elizabeth J. Opila*
Department of Chemical Engineering
Cleveland State University
Cleveland, OH 44115

At high temperatures SiC and Si_3N_4 react with water vapor to form a silica scale. Silica scales also react with water vapor to form a volatile $Si(OH)_4$ species. These simultaneous reactions, one forming silica and the other removing silica, are described by paralinear kinetics. A steady state, in which these reactions occur at the same rate, is eventually achieved. After steady state is achieved, the oxide found on the surface is a constant thickness and recession of the underlying material occurs at a linear rate. The steady state oxide thickness, the time to achieve steady state, and the steady state recession rate can all be described in terms of the rate constants for the oxidation and volatilization reactions. In addition, the oxide thickness, the time to achieve steady state, and the recession rate can also be determined from parameters that describe a water vapor-containing environment. Accordingly, maps have been developed to show these steady state conditions as a function of reaction rate constants, pressure, and gas velocity. These maps can be used to predict the behavior of silica-formers in water-vapor containing environments such as combustion environments. Finally, these maps are used to explore the limits of the paralinear oxidation model for SiC and Si_3N_4.

INTRODUCTION

SiC and Si_3N_4 are proposed for long-term applications in combustion environments. Some of these applications include combustor liners and turbine vanes for both propulsion and power generation. The combustion environment for hydrocarbon/air systems contains about 10% water vapor, independent of hydrocarbon type and fuel-to-air ratio (1). The reactions of SiC and Si_3N_4 with water vapor are therefore a concern. While much of the information in this paper is generic for any environment containing water vapor, this paper will emphasize the combustion environment in a gas turbine since the work summarized here was driven by development for these applications.

In water vapor-containing environments SiC and Si_3N_4 undergo both an oxidation and a volatilization reaction, as shown below for SiC:

$$SiC + 3H_2O(g) = SiO_2 + 3H_2(g) + CO(g) \quad [1]$$

$$SiO_2 + 2H_2O(g) = Si(OH)_4(g) \quad [2]$$

* Resident at NASA Glenn Research Center, Cleveland, OH 44135

The kinetics of the oxidation reaction are described by the parabolic rate constant for oxide formation, k_p, whereas the kinetics of the volatilization reaction are described by the linear rate constant for oxide volatilization, k_l. These reactions occur simultaneously and are described by paralinear kinetics. The paralinear kinetic model has been developed for simultaneous oxidation and volatilization of chromia-formers by Tedmon (2) and is directly applicable to the oxidation of silica-formers in water vapor:

$$\frac{dx}{dt} = \frac{k_p}{2x} - k_l \qquad [3]$$

where x is oxide thickness and t is time. At long times or high volatility rates a steady state is achieved in which oxide is formed at the same rate it is volatilized. SiC and Si_3N_4 undergo linear recession, given by the rate $\dot{y}_L$, when this steady state is achieved which is directly related to the volatility rate of the oxide, k_l. Dimensional changes due to paralinear oxidation are shown as a function of time for SiO_2 growth on SiC in Figure 1. At steady state, a limiting oxide thickness, x_L, is achieved which is given by (2):

$$x_L = \frac{k_p}{2k_l} \qquad [4]$$

The subscript L here and in all future uses refers to the steady state limit. The paralinear oxidation kinetics of SiC and Si_3N_4 in water vapor and combustion environments have been studied under a wide variety of conditions (3-10), and the model has been shown to be valid in a majority of cases. It is therefore timely to extend the description of steady state oxidation/volatilization kinetics and compare the theory to observations obtained for SiC and Si_3N_4 over a wide range of experimental conditions. This work was begun in a previous paper (11) but is more completely addressed herein.

Specifically, the aims of this paper are as follows. First, the concept of the time to reach steady is state is developed to extend Tedmon's treatment of paralinear kinetics. Second, general relationships for limiting oxide thickness, the time to reach steady state and steady state recession rate are developed in terms of the total pressure, gas velocity and temperature in the combustion environment. Third, a series of constant temperature maps are presented which graphically show the variation of the steady state oxide thickness, time to reach steady state, and steady state recession rate with both rate constants and combustion environment parameters. Experimental results are then compared to theoretical predictions. Finally, these maps are used as a framework for discussing the limitations of the paralinear oxidation model for SiC and Si_3N_4 in combustion environments.

DETERMINATION OF THE TIME TO ACHIEVE STEADY STATE

In Tedmon's treatment of paralinear kinetics, the steady state oxide thickness, as well as the steady state recession rate, are described mathematically (2). While the time to reach

95% of the limiting oxide thickness is shown graphically for a real chromia former as a function of temperature, a mathematical expression was not developed. In describing paralinear kinetics for a system, the time to reach steady state is essential for predicting when the steady state oxide thickness is formed, as well as when a simple linear rate describes the recession of the underlying material. In order to determine the change in oxide thickness with time, the integrated form of Equation 3 is needed. This expression is:

$$t = \frac{k_p}{2k_l^2}\left[-\frac{2k_l}{k_p}x - \ln\left(1-\frac{2k_l}{k_p}x\right)\right] \qquad [5]$$

Upon inspection of this equation as well as Figure 1, it can be seen that the oxide thickness, x, approaches the limiting thickness, x_L, given by Equation 4, asymptotically with time. An expression for the time at which the limiting oxide thickness is achieved cannot be defined. Instead, as is typical for this kind of a function, a time constant can be defined which is that time at which the oxide thickness given by parabolic kinetics (valid at short times) is equal to the oxide thickness found at steady state oxidation/volatilization (valid at long times). This time constant then defines the transition time at which the simple parabolic oxidation model becomes less accurate than the simple steady state oxidation/volatilization model. The graphical determination of the time constant for establishing a limiting oxide thickness, $t_{c,o}$, is shown in Figure 2 and is given by:

$$t_{c,o} = \frac{k_p}{4(k_l)^2} \qquad [6]$$

In Figure 2, both the oxide thickness and time have been normalized by the values x_L and $t_{c,o}$ so this figure is general for any rate constants, k_p and k_l. Independent of rate constants, the time constant represents that time at which the oxide thickness is 70% of the limiting oxide thickness, x_L. In order to define a time to form an oxide thickness that is closer to the limiting oxide thickness, some multiple of the time constant t_{co} must be used. For example, for the purposes of this paper it was decided that a multiple of 2 x $t_{c,o}$, which represents the time to reach 84% of the limiting oxide thickness, is a better description of the time to reach nearly steady state oxidation/volatilization. This time has been defined as the limiting time, t_L, i.e.:

$$t_L = \frac{k_p}{2(k_l)^2} \qquad [7]$$

A table is included in Figure 2 that shows the multiples of the time constant that correspond to the time to form a certain percentage of the limiting oxide thickness.

Similarly, a time constant can be formulated to describe the time to achieve steady state recession. In this case, the time constant is defined as that time at which the expression for parabolic recession (valid at short times) intersects with the expression for linear recession (valid at long times). This time constant then defines the transition time at which the simple parabolic recession model becomes less accurate than the simple steady state recession model. The graphical determination of the time constant for establishing a steady state recession rate, $t_{c,r}$, is shown in Figure 3 and is given by:

$$t_{c,r} = \frac{k'_p}{(k'_l)^2} \qquad [8]$$

Here k'_p and k'_l represent the rate constants for parabolic and linear recession of SiC. (These are different from the rate constants for parabolic oxidation and linear volatilization of SiO_2 used in Equations 3 through 7. The units k'_p and k'_l are in μ^2/h and μ/h of SiC or Si_3N_4 consumed rather than μ^2/h and μ/h of SiO_2 formed or volatilized as in Equations 3 through 7. The rate constants are related by the molecular weights and densities of silica and the underlying material as shown in the next section.) Here, both the recession depth and time have been normalized by y_n and $t_{c,r}$. The quantity y_n is given by k_p'/k_l' and is somewhat arbitrarily chosen. Figure 3 is then general for any rate constants k_p' and k_l'. Figure 3 contains a table that shows the multiples of the time constant that correspond to the time at which the recession rate corresponds to a percentage of the steady state linear recession rate. At one time constant, for example, the observed recession rate for paralinear oxidation/volatilization is 85% of that which would be found at steady state oxidation/volatilization. For the purposes of this paper one time constant has been chosen as an adequate description of the time to reach nearly steady state linear recession rates.

PARAMETRIC EXPRESSIONS FOR OXIDATION AND VOLATILIZATION

In the previous sections the steady state oxide thickness, the time constant to reach steady state, and the recession rate have been shown to depend on the oxidation rate as well as the volatilization rate. It is also useful to understand how the oxidation/volatilization processes in turn depend on more fundamental parameters (pressure, water vapor partial pressure, gas velocity and temperature) that describe any environment, rather than on empirical kinetic rate constants that may or may not be known. In order to understand how the limiting oxide thickness, time constant and recession rate depend on these parameters, the parametric expressions for the rate constants must be known. These are discussed in the following sections.

Parametric Expression for the Parabolic Oxidation Rate Constant

The parabolic rate constant describes the kinetics of Equation 1 for moderately thick scales (diffusion limited growth). This rate constant varies with the water vapor partial pressure and temperature but is independent of gas velocity. The temperature

dependence will be discussed later. The water vapor dependence can be described using a power law:

$$k_p \propto P_{H_2O}^n \quad [9]$$

where n is the power law exponent. This power law should be identical for all silica – formers since parabolic oxide growth is rate limited by transport of oxidant through the silica scale. Deal and Grove (12) observed a power law exponent of unity for the parabolic oxidation of silicon by water vapor, indicating that the oxidation reaction is limited by the diffusion of molecular water, rather than a charged species, through the silica scale. Studies on the oxidation of SiC in water vapor found power law exponents varying between 0.76 and 0.91 (13,14). These parameters are summarized in Table 1. Studies on the diffusivity of water vapor in silica also find that molecular water vapor is the diffusing species (15). For the purposes of this study a power law exponent of one will be used to describe the water vapor partial pressure dependence of the parabolic oxidation rate constant for SiC and Si_3N_4. Using results obtained for SiC oxidation at 1316 °C (13) the following expression is used in this paper to extrapolate oxidation rates in water vapor for silica formers:

$$k_{p,1316°C} = 0.44\, P_{H_2O}^1, \ [\mu^2\ SiO_2/h] \quad [10]$$

This temperature was chosen as a reference temperature since this is the only temperature where a complete data set is available for both rate constants.

Parametric Expression for the Linear Volatilization Rate Constant

The linear volatilization rate constant describes the kinetics of Equation 2. This rate constant varies with the water vapor partial pressure, total pressure, temperature and gas velocity. The temperature dependence will be discussed later. Under combustion conditions, the volatilization of silica to form $Si(OH)_4$ is limited by transport of $Si(OH)_4$ through a laminar gaseous boundary layer. This rate is given by the following expression for a flat plate geometry:

$$k_l = 0.664\, Re^{1/2}\, Sc^{1/3}\, \frac{D\rho_v}{L} \quad [11]$$

where Re is the dimensionless Reynold's number, Sc is the dimensionless Schmidt number, D is the interdiffusion coefficient of $Si(OH)_4$ in the boundary layer gas, ρ_v is the equilibrium concentration of the volatile $Si(OH)_4$, and L is a characteristic length. This equation can be further expanded:

$$k_l = 0.664 \left(\frac{Lv\rho}{\eta}\right)^{1/2} \left(\frac{\eta\rho}{D}\right)^{1/3} \frac{D\rho_v}{L} \quad [12]$$

where v is the gas velocity, η is the gas viscosity, and ρ is the concentration of the boundary layer gas. This expression can then be simplified to the combustion environment parameters of pressure and velocity:

$$k_l \propto \frac{v^{1/2} P_{Si(OH)_4}}{P_{total}^{1/2}} \qquad [13]$$

and knowing that $P_{Si(OH)_4}$ is proportional to $P_{H_2O}^2$ from Equation 2, and P_{H_2O} is equal to about 0.1 P_{total} for combustion environments as discussed in the introduction, then:

$$k_l \propto v^{1/2} P_{total}^{3/2} \qquad [14]$$

Remarkable agreement between the empirical results and boundary layer transport model has been found (7,8). The measured dependencies of volatilization are also summarized in Table 1. Using results obtained for SiC oxidation/volatilization at 1316 °C (7) the following expression is used in this paper to extrapolate oxidation rates in water vapor for silica formers:

$$k_{l,1316°C} = 0.36 \frac{P_{H_2O}^2}{P_{total}^{1/2}} v^{1/2} \text{ , [}\mu \text{ } SiO_2/h] \qquad [15]$$

The pressure dependence will vary, of course, in conditions where other volatile species such as SiO(g), $SiO(OH)_2$(g), or SiO(OH)(g) are more stable (8).

Parametric dependence of limiting oxide thickness, time constant, and recession rate

It is now straightforward to substitute the parametric dependence of the oxidation and volatilization rate constants (Equations 10 and 15) into the previous expressions for x_L and t_L (Equations 4 and 7) to derive the following expressions:

$$x_{L,1316°C} = 0.615 \frac{P_{total}^{1/2}}{P_{H_2O} v^{1/2}} \text{ , [}\mu \text{ } SiO_2] \qquad [16]$$

And for hydrocarbon combustion environments where P_{H_2O} is 0.1 P_{total}, the following general relationship holds true:

$$x_L \propto (P_{total} v)^{-1/2} \qquad [17]$$

The steady state oxide thickness therefore decreases with both pressure and gas velocity. Similarly,

$$t_{L,1316°C} = 1.71 \frac{P_{total}}{P_{H_2O}^3 \, v}, \text{ [h]} \qquad [18]$$

And again, for hydrocarbon combustion environments where P_{H_2O} is 0.1 P_{total}, the following general relationship holds true:

$$t_L \propto \left(P^2 \, v\right)^{-1} \qquad [19]$$

The time to achieve steady state also decreases with both pressure and gas velocity.

As stated earlier, the steady state recession rate, $\dot{y}_L$, is directly proportional to the volatility rate of silica, k_l, and is given by:

$$\dot{y}_L = k_l \frac{\rho(SiO_2)}{MW(SiO_2)} \frac{MW(SiC)}{\rho(SiC)} \qquad [20]$$

Here ρ is the density and MW is the molecular weight of the indicated species. The exact semi-empirical relationship for $\dot{y}_L$ is:

$$\dot{y}_{L,1316°C} = 0.18 \frac{P_{H_2O}^2 \, v^{1/2}}{P_{total}^{1/2}}, \text{ [}\mu\text{ SiC/h]} \qquad [21]$$

And again, for hydrocarbon combustion environments where P_{H_2O} is 0.1 P_{total}, the following general relationship holds true:

$$\dot{y}_L \propto P^{3/2} \, v^{1/2} \qquad [22]$$

For easy reference the general expressions for the steady state conditions are summarized in Table 2.

CASE STUDIES FOR PARALINEAR OXIDATION OF SiC AND Si_3N_4

Up to this point the theoretical expressions for paralinear oxidation and volatilization; the parametric dependence of the steady state oxide thickness, time constant, and recession rate; as well as semi-empirical expressions at 1316 °C have been developed. It is now

appropriate to introduce a number of studies that have been conducted over a wide range of conditions that will be compared to the theory in the remainder of this paper. These case studies include three furnace studies (3-5) as well as three studies in actual combustion environments (6,7,10). The test parameters for each of these studies are listed in Table 3. The results obtained in a high-pressure burner rig at NASA Glenn (7) were used to establish the empirical constants for Equations 16, 18, and 21, although the parametric dependence in these equations is derived from theory (and verified by the experimental observations). This is not a complete list of studies that describe the paralinear oxidation/volatilization of silica-forming materials. Other excellent studies can be found in References 17 and 18. The conditions for these studies are similar to those in Reference 7, thus they were not included in the case studies.

LIMITING OXIDE THICKNESS AND TIME CONSTANT MAPS IN TERMS OF RATE CONSTANTS

The concept of an oxide thickness map can first be developed in terms of, k_p, the parabolic oxidation rate constant and, k_l, the linear volatilization rate constant. This is shown in Figure 4, calculated for SiC at 1316°C. Each diagonal line is a line of constant limiting oxide thickness. Thus for a given oxidation rate and a given volatilization rate, the steady state oxide thickness at 1316°C can be picked directly from this map. A number of points are shown on this map that plot limiting oxide thickness for each case study. Steady state oxide thicknesses were calculated using Equation 4. Experimentally determined rate constants were not available in all cases, so to be consistent, calculated rate constants were used in all cases. Rate constants were calculated using Equations 10 and 15 and the experimental parameters in Table 3. Calculated rate constants are compared to those experimentally measured in Table 4. In most cases there is very good agreement between calculated and observed rate constants. This comparison will be discussed in greater detail in a following section.

Similarly, a steady state time constant map as a function of rate constants is shown in Figure 5. Here again, rate constants for each case study are calculated from Equations 10 and 15 based on parameters in Table 3 and are used in Equation 7 to plot steady state time constants. Each diagonal line is a line of constant time to reach steady state. Thus for a given oxidation rate and a given volatilization rate, the steady state time constant for SiC at 1316°C can be picked directly from this map.

It is unnecessary to construct a map of steady state recession as a function of rate constants since it depends on the linear volatilization rate of silica alone.

These two maps, Figures 4 and 5, demonstrate a number of concepts. First, these maps allow easy visualization of the competition between oxide growth and oxide volatilization and the effects on the expected surface oxide thickness as well as the rate at which the steady state paralinear process is approached. Second, the case studies really cover a wide range of rate constants and this will allow limits for the paralinear model to be explored in detail. Third, the time constant is much more sensitive to changes in rate

constant than the limiting oxide thickness. Time constants vary from 2 minutes to $4x10^5$ hours. This is seven orders of magnitude variation in time to reach steady state. The limiting oxide thickness varies by three orders of magnitude in this same rate constant space. Finally, these maps show that it may be more useful to think of how the limiting oxide thickness, time constant, and steady state recession rate vary with parameters that describe the combustion environment. Experimentally determined rate constants are not always available. In addition, these maps do not help to visualize how the paralinear process is affected by changes in pressure or gas velocity. The development of maps as a function of pressure and velocity is the topic of the next section.

LIMITING OXIDE THICKNESS, TIME CONSTANT, AND RECESSION RATE MAPS IN TERMS OF TOTAL PRESSURE AND GAS VELOCITY

The concept of oxide thickness maps, first developed in terms of the oxidation and volatilization rate constants, can now be extended to the parametric expression developed in Equation 16 above. Figure 6 shows the limiting oxide thickness contours calculated for SiC at 1316°C as a function of total pressure and gas velocity. Each diagonal line is a line of constant limiting oxide thickness. Thus for a given total pressure and a given gas velocity, the steady state oxide thickness for SiC at 1316°C can be picked directly from this map. The points shown on this map plot actual gas pressures and velocities for five case studies for SiC or Si_3N_4 exposures in experimental or combustion environments with the steady state oxide thickness calculated using Equation 16. (The case study for laboratory furnace 2 is omitted on these maps since the simplification that $P_{H_2O} = 0.1$ P_{total} can not be made for these test conditions. In addition, it was assumed the water vapor partial pressure in the high pressure furnace was 1 atm so that the assumption that $P_{H_2O} = 0.1$ P_{total} could be made for this case.)

Similarly, maps for time to reach steady state and steady state recession rate as a function of total pressure and gas velocity calculated for SiC at 1316°C are shown in Figures 7 and 8, respectively. These maps were calculated using Equations 18 and 21. The points on these maps again represent the actual total pressure and gas velocity for the five case studies.

While these maps (Figures 6 through 8) give less information about the competing silica formation and removal processes in the paralinear mechanism than Figures 4 and 5, they do allow easy visualization of the effects of changes in total pressure and gas velocity on the expected surface oxide thickness, the rate at which the steady state paralinear process is approached, and the steady state recession rate of structural material. Again, these maps demonstrate that the steady state time constant is most sensitive (closely spaced contours) to changes in pressure and gas velocity, the recession rate has intermediate sensitivity, and the limiting oxide thickness is least sensitive to changes in combustion gas parameters.

COMPARISON OF EXPERIMENTAL RESULTS TO THE PARALINEAR MODEL

Rate constants

As mentioned earlier, the measured and calculated rate constants are compared in Table 4. In general there is very good agreement. The rate constants measured for SiC in all cases are within a factor of two of the calculations based on the semi-empirical expression from the high pressure burner rig results at 1316°C, Equations 10 and 15. Several points should be made. First the experimental rates were obtained at various temperatures as reported in Table 3, whereas all calculated rates are for 1316°C. Nevertheless the agreement is quite good indicating the empirically derived constants in Equations 10 and 15, as well as the parametric dependence, work well over a wide range of conditions. Second, the mechanism for oxidation in the high pressure furnace can not be described using a parabolic rate constant due to the porous oxide morphology formed (see Figure 9c), so this case is not well represented by paralinear kinetics. This case will be discussed in more detail in the following sections. The good agreement between calculated and measured rate constants in the majority of the cases gives confidence that the derivations of limiting oxide thickness, time constant, and steady state recession rate that are based on these rate constants can be used to make accurate predictions of paralinear oxidation/volatilization behavior.

Limiting Oxide Thickness

Figure 9 shows cross-sections of oxides formed on SiC or Si_3N_4 for each case study shown in Table 3. Table 5 summarizes these findings as well as the predicted limiting oxide thickness for each case study.

The oxide grown on SiC in laboratory furnace 1 (Figure 9a) is about 2 μm thick. This is much less than the calculated limiting oxide thickness of 91 μm, however, the exposure time is only 100 hours which is only a miniscule fraction of the time required to achieve steady state. The oxidation kinetics in this case were well modeled by parabolic kinetics alone since the volatility of silica is negligible.

The oxide grown on SiC in laboratory furnace 2 (Figure 9b) is, on average, about a factor of two less than the predicted limiting oxide thickness. The exposure time was one-third the time to achieve steady state. These results are in good agreement with expectations. In this case, the full paralinear model is needed to model the observations. Both the oxidation rate and the volatility rate are needed to model the observed kinetics.

Figure 9c shows the oxides grown on both SiC and Si_3N_4 in the high-pressure furnace environment. There are several phenomena that must be considered when comparing the observed oxide thickness to the predicted limiting oxide thickness. First, the gas velocity in this furnace is nearly stagnant (0.05 cm/sec). Silica volatility will be negligible in this case. This can be observed quite readily from Figure 4, where the oxidation rate is quite high due to the high water vapor partial pressure, but the volatility rate is quite low due to the very low gas velocity. In this case, it would be expected that parabolic kinetics alone

would be sufficient to model the observed oxide growth. This brings up the second phenomenon that must be considered. From Equation 10, it is shown that the parabolic oxidation rate has a strong dependence on the water vapor partial pressure. As the oxidation rate increases, the rate of production of gaseous oxidation products also increases as can be seen from the oxidation reaction (Equation 1). The high pressures of these gases generate porosity in the oxide layer as shown in Figure 9c for SiC. The amount of pores in the silica scale has been shown to increase with water vapor partial pressure (14). Because the scale is no longer dense, the transport path length of water vapor through the silica scale is no longer parabolically increasing. Gas phase transport can now occur through the interconnected cracks and pores. The oxide growth rate is limited by solid state transport of water vapor through the dense portion of the silica scale near the interface which remains at a nearly constant thickness with time (5). The oxidation kinetics and corresponding recession rates are therefore linear. In the case of the Si_3N_4 exposed in the high pressure furnace, the dense layer is much thicker presumably due to the relatively lower amount of gaseous products released per mole of silica formed. In this case, parabolic kinetics were observed. The surface layer of oxide is still porous and friable. At long times, spallation of this porous surface layer may limit the thickness of the silica rather than volatility. It remains to be demonstrated if there is some upper limit of silica thickness at which spallation typically occurs. The important point to take away from these exposures is that the underlying material and the resulting oxide morphology affect the kinetic rate law applicable to oxide growth. A paralinear oxidation/volatilization model is not applicable for the conditions in the high pressure furnace.

Figure 9d and 9e show the oxide morphology found for SiC exposed in a mach 0.3 burner rig and a high pressure burner rig, respectively. In both cases, the predicted steady state oxide thickness is less than that actually observed. This could be explained by impurity-enhanced oxidation. It is known that even small amounts of impurities can increase the oxidation rate of SiC by an order-of-magnitude (19). Burner rigs and other real combustion environments do contain more impurities than laboratory furnaces. If impurity effects caused k_p to increase by an order-of-magnitude over the rate given by Equation 10, then the limiting oxide thickness would be 6μm in both cases. This is in good agreement with observations for oxides formed in both burner rigs.

Figure 9f shows a cross-section of a Si_3N_4 vane exposed in an industrial turbine. No oxide is visible on the surface. The surface roughness appears to correspond to the shape of individual Si_3N_4 grains with the grain boundary phase removed. The gas velocity in this environment is much higher than found in the other case studies. Again several phenomena must be considered when comparing the predicted limiting oxide thickness to the lack of oxide actually observed. First, for very thin silica layers, parabolic oxidation kinetics is not expected. The chemical reaction rate of the water vapor with the underlying material could be expected to control the oxidation rate since transport across a thin layer would be rapid. In this case, linear oxidation rates would be observed. Secondly, because the volatilization rate is so rapid and the time to reach steady state is so short, the oxidation rate is only of interest at very short times for an oxidation/volatilization mechanism rendering the first point of little interest. Third, if the

volatilization is so rapid that no oxide is found on the surface, the kinetics of recession may not even be related to the volatility of silica. Several scenarios can be envisioned. The recession could be controlled by the rate of chemical reaction of the oxidant with the SiC or Si_3N_4 to form silica. As soon as oxide is formed it is swept away. Another possibility is that a different reaction sequence occurs rather than the reactions in Equations 1 and 2. Some kind of "active" volatilization could occur similar to the active oxidation mechanism that occurs for silica-formers at low oxygen partial pressures. In the case of active oxidation at low oxygen partial pressures, SiC reacts with oxygen to form SiO(g) rather than SiO_2. An analogous reaction can be envisioned in which SiC reacts directly with water vapor to form $Si(OH)_4(g)$ without the intermediate silica formation step. It might be possible to distinguish this kind of reaction by determining the temperature dependence of recession. It would be difficult to perform these kinds of experiments since these very high gas velocities found in the turbine cannot be readily obtained in a laboratory or rig environment. The important point to take away from these turbine exposures is that a paralinear oxidation/volatilization model is not applicable for very high velocity conditions where the silica volatilization rate exceeds the silica formation rate.

Steady State Recession Rate

Steady state recession rates calculated from Equation 21 are shown in Table 6. While sufficient data are available to compare experimentally observed oxide thicknesses with predicted limiting oxide thicknesses, the same is not true for recession rates. Recession by paralinear oxidation/volatilization is too small to be measurable in reasonable amounts of time for the furnace studies and the mach 0.3 burner rig. Given a one hundred hour test and the calculated rates listed in Table 6, recession would only be measurable (>25μm) for exposures in the high-pressure burner rig and the industrial turbine.

Material recession has been measured for the materials tested in the high-pressure furnace, but as already discussed, this recession can be attributed to consumption of material by a linear oxidation mechanism for SiC and parabolic oxidation which may be limited by spalling for Si_3N_4 since volatilization of silica is minimal.

Equation 21 was determined from the high-pressure burner rig results, so an independent comparison cannot be made in this case. However, the good agreement between the predicted parametric dependence of the recession rate (Equation 14) and the observed recession rate dependence in Equation 21 provides some measure of confidence that this equation is correct. In addition, the recession measured for silica formers in other pressurized burner rig studies (17,18) is in good agreement with Equation 21 for moderately different conditions.

Finally, the calculated rates are in good agreement with the measured rates for the Si_3N_4 exposed in the turbine. Because no silica was observed on the surface of the Si_3N_4 vane, the paralinear oxidation/volatilization model should not be applicable. However, the good agreement of calculated and predicted steady state recession rates may indicate that the conditions under which the vane was exposed are just at the limit where the paralinear

model may be applied; i.e., at lower volatility rates paralinear kinetics apply and at higher volatility rates some of the mechanisms described above in the limiting oxide thickness section may be operative.

While recession rates are difficult to measure when volatilization is only moderately rapid, linear weight losses that correspond to the linear recession rates are quite easily obtained. The volatilization rate constants shown in Table 4 were obtained by weight measurements for cases B, D and E. Measured weight loss and material recession were both obtained in the high pressure burner rig and were found to differ by a factor equal to the density of SiC, as expected.

TEMPERATURE DEPENDENCE OF PARALINEAR OXIDATION - VOLATILIZATION

Maps for limiting oxide thickness, time constant, and steady state recession rate as a function of rate constants or pressure/velocity space are calculated at a single temperature. Different maps must be calculated for each temperature. Up to this point, all calculations have been limited to one temperature, 1316°C, and the temperature dependence has been neglected. This has been done because oxidation and volatilization rate constants measured as a function of pressure and gas velocity for a single material in a single rig are not available over a range of temperatures. The available measured temperature dependencies of the rate constants are summarized in Table 1. The temperature dependence for both rate constants determined in a single study can be found only for SiC studied in a laboratory furnace (4) and the uncertainties of the temperature dependence in this study are quite large. One point to note is that the enthalpies for oxidation and volatilization are similar, so predicting the temperature dependence of the limiting oxide thickness and the time to reach steady state, which depend on both k_p and k_l is difficult. However, when good oxidation/volatilization results over a wide range of temperatures become available for a given material the following discussion will be applicable.

The temperature dependence of the parabolic rate constant arises from the enthalpy of diffusion for molecular water in silica. The values reported for this oxidation enthalpy, $\Delta H_{ox,}$ in the literature are summarized in Table 1 and range from 28 to 156 kJ/mol. The temperature dependence of the volatilization reaction arises mainly from the enthalpy of Reaction 2. This temperature dependence is found in the ρ_v term in Equations 11 and 12 which arises from the temperature dependence of the $P_{Si(OH)_4}$ term in Equation 13. The enthalpy for volatilization, ΔH_{vol}, varies between 3 and 108 kJ/mol as reported in the literature and summarized in Table 1. Thus the temperature dependence of these two mechanisms may be similar.

The temperature dependence of the steady state oxide thickness is given by:

$$x_L = \frac{k_p}{2k_l} \propto \exp\left(\frac{\Delta H_{vol} - \Delta H_{ox}}{RT}\right) \quad [23]$$

where ΔH is the enthalpy, the subscript *vol* indicates volatilization, the subscript *ox* indicates oxidation, R is the gas constant, and T is absolute temperature. In reference 4, ΔH_{vol} = 3±75 kJ/mol and ΔH_{ox} = 35±147 kJ/mol. Thus it is highly uncertain which enthalpy is larger. If, in fact, $\Delta H_{vol} < \Delta H_{ox}$, then x_L increases as T increases. This discussion assumes the major volatile species is $Si(OH)_4(g)$. At high temperatures (≥1400°C) $SiO(OH)_2(g)$ or $SiO(OH)(g)$ species may be important (8). These species have much higher enthalpies of formation from silica and water vapor. In these cases the volatilization reaction would become increasingly important as the temperature was increased. The steady state oxide thickness might therefore decrease with temperature. There are no oxide thickness measurements available to see how the steady state oxide thickness varies with temperature.

Similarly, the temperature dependence of the time to reach steady state is given by:

$$t_L = \frac{k_p}{2k_l^2} \propto \exp\left(\frac{2\Delta H_{vol} - \Delta H_{ox}}{RT}\right) \quad [24]$$

where all terms have been previously defined. Again, assuming $2\Delta H_{vol} < \Delta H_{ox}$ based on reference 4, then t_L will increase as T increases. Clearly, these temperature trends will depend on the material of interest and cannot be predicted without better data.

Finally, the temperature dependence of the steady state recession rate will depend only on the enthalpy of volatilization and it is quite straightforward to state that recession rates increase exponentially with temperature.

LIMITS OF THE PARALINEAR MODEL FOR SiC AND Si_3N_4 OXIDATION - VOLATILIZATION IN COMBUSTION ENVIRONMENTS

The maps developed in Figures 6, 7, and 8 provide a framework for understanding the limits of the paralinear model. Several points have been made in the previous discussion about the applicability of the paralinear oxidation and volatilization model for silica-forming materials in the specific case studies. These points are summarized below and in Table 7. A general map, shown in Figure 10, is then developed to show approximate pressure and gas velocity limits for applying the paralinear model. Some of these limits are based on the long-term application (10^4 to 10^5 hours) of SiC and Si_3N_4 in a combustion environment. Clearly different limits would be chosen for significantly different applications.

1. Negligible volatilization/recession

At low gas velocities and low pressures in a combustion environment, silica volatilization and the corresponding steady state recession rate are negligible. Parabolic oxidation kinetics are sufficient to model the oxide growth and recession. In Figure 10, a steady state recession rate of 1×10^{-3} μ/h has been chosen as negligible. For recession rates larger than this, the paralinear model should be used.

2. Long time constant

At low gas velocities and low pressures in a combustion environment, the time to reach steady state oxidation and volatilization can be as long as the expected use life of a component. Clearly it is not necessary to apply paralinear kinetics to model the oxidation of materials under these conditions. In Figure 10, a time constant of 10^4 hours was chosen as a limit for application of the paralinear model. For shorter time constants, the paralinear model should be used.

3. Negligible volatilization, high oxidation rate

At low gas velocities and high pressures in a combustion environment the volatilization rate is low. The oxidation rate is high due to the high water vapor partial pressure. While paralinear kinetics can still be used to model the oxidation and volatilization reactions under these conditions, the kinetics are dominated by the oxidation reaction and can therefore be modeled by the oxide growth kinetics alone. In addition, because oxidation rather than volatilization dominates the reaction kinetics, the observed oxidation behavior is material dependent. In volatility-dominated conditions (high gas velocity), the volatilization of silica appears to be independent of the underlying material or the purity of the silica. However, when the kinetics are dominated by high oxidation rates, as they are at low gas velocities and high water vapor partial pressures, the oxidation rate and mechanism are affected by the underlying material. The purity of the material and the product gases generated by the oxidation reaction affect the oxidation mechanism. This is evident from the different behavior observed for SiC and Si_3N_4 in the high pressure furnace (Figure 9c). These differences in oxidation mechanism are now discussed.

3a. *Nonprotective scale*

For SiC exposed under low gas velocity, high pressure conditions for 500h, a thick porous scale was formed with a 5 micron thick dense silica layer near the oxide/SiC interface (5). This dense layer did not grow with time, and the observed kinetics were linear. The following mechanism explains these observations. The high oxidation rates which occur at high water vapor partial pressures generate large amounts of product gases (CO and H_2). These gases form bubbles and pores in the silica scale (5, 14). The oxidation rate is limited by transport of water vapor through the 5 micron thick dense layer of silica near the oxide interface. Thus, a 5 micron steady state oxide thickness has been chosen as a limit for the paralinear model in Figure 10. For SiC, only conditions which result in a steady state oxide thickness less than 5 microns can be modeled by paralinear kinetics (or simple parabolic kinetics). Oxides thicker than 5 microns would be full of bubbles and pores and grow by linear kinetics.

3b. *Thick spalling scale*

For Si_3N_4 exposed under low gas velocity, high pressure conditions for 500h, 20-25 μm thick scales were formed which had very friable surface layers (20). The oxidation kinetics for Si_3N_4 oxidized under these conditions were parabolic. The friable surface layer indicates that spallation will be a problem for very thick oxides. If spallation occurs at some limiting thickness, then kinetics would be parabolic (as a simple case of oxidation/volatilization paralinear kinetics) until this oxide thickness is achieved. It is possible that as the scale grows thicker, the surface layer spalls off to some average thickness. This remains to be verified. If spallation of thick scales occurs, then the paralinear oxidation/volatilization model would not be applicable for predicted steady state oxide thicknesses greater than the spallation limiting value. In Figure 10, a spallation limited oxide thickness of 30 μm has been chosen as a limit for the paralinear oxidation/volatilization model. For thicker oxides, a paralinear oxidation/spallation model might be a valid. Oxidation/spallation models have been used to describe the kinetics of cyclic oxidation of superalloys (21) for many years. A better understanding of silica scale growth in high pressure water vapor for very thick scales is needed.

4. Thin or missing scale

At high pressures and high gas velocities in a combustion environment silica volatilization rates are more rapid than oxidation rates. Very thin scales are formed or bare surfaces are observed. The rate limiting mechanism is unknown under these conditions and may be any of the following as discussed in more detail above: linear oxidation with simultaneous linear volatilization for thin scales, volatilization limited by the oxidation rate, or an active volatilization process in which the silicon-based ceramic reacts directly to form a volatile hydroxide. In Figure 10, a steady state oxide thickness of 0.1 micron has been chosen as the limit for paralinear oxidation/volatilization. For steady state oxide thicknesses larger than this, the paralinear model is applicable.

The combination of all the limits discussed in the four points above maps out a region in which the paralinear model for oxidation/volatilization can be applied. In this region, the equations summarized in Table 2 are valid. It should be noted that the high-pressure boundaries at both very high and very low gas velocities are tentative due to the limited number of conditions under which SiC or Si_3N_4 have been tested. The positions of these lines are indeterminate, although the slopes should be valid. More testing is needed before these boundaries can be definitively established. Many of the propulsion and power generation applications for SiC and Si_3N_4, however, do operate in the pressure and gas velocity space mapped out by the paralinear regime shown in Figure 10. The mach 0.3 burner rig and high pressure burner rig both fall within this regime and are therefore good tools for screening materials for long-term applications in combustion environments where paralinear oxidation/volatilization occurs.

SUMMARY AND CONCLUSIONS

Steady state paralinear oxidation and volatilization of SiC and Si_3N_4 in combustion environments can be summarized by the relationships given in Table 2. It is important to

characterize the oxide morphology in order to understand the steady state recession mechanisms and rates. Time constants to achieve steady state are very sensitive to small changes in reaction rate and hence small changes in pressure and gas velocity. Linear volatilization rate constants are sufficient to define the steady state recession rate of silica formers in combustion environments when in the paralinear regime. Steady state oxide thickness, time constant, and recession rate maps allow prediction of SiC and Si_3N_4 behavior in combustion environments. These maps also provide a framework for understanding the limits of the paralinear model. Additional characterization of oxidation/volatilization of silica formers is needed to establish the temperature dependence of the process. Finally, more studies are needed to understand the chemical degradation mechanisms of silica formers in high pressure and very high gas velocity combustion environments.

ACKNOWLEDGMENTS

The author would like to acknowledge the contributions of co-workers at the NASA Glenn Research Center: Dennis Fox, Nathan Jacobson, Craig Robinson, and Jim Smialek were all part of the Environmental Durability team studying the chemical durability of SiC and Si_3N_4 in combustion environments. Special thanks to Jim Smialek for his careful review of this paper. In addition, Mike Cuy, Raiford Hann (now at ITT Technical Institute, Rancho Cordova, CA), Barry Licht (retired) and Carl Stearns (retired) all had critical contributions to this work. The author would also like to thank Karren More and Peter Tortorelli of Oak Ridge National Laboratory for sharing results from the high pressure furnace. Finally, the author would like to thank Richard Wenglarz, formerly of Allison Engine Corporation (now at South Carolina Institute for Energy Studies, Clemson, SC) for providing a Si_3N_4 vane for study. This work was performed as part of the Enabling Propulsion Materials Program for the High Speed Research Program.

REFERENCES

1. N.S. Jacobson, "Corrosion of Silicon-Based Ceramics in Combustion Enviornments," J. Am. Ceram. Soc., 76 [1] 3-28 (1993).
2. C.S. Tedmon, Jr., "The Effect of Oxide Volatilization on the Oxidation Kinetics of Cr and Fe-Cr Alloys," J. Electrochem. Soc., 113 [8] 766-68 (1967).
3. E.J. Opila, "Oxidation Kinetics of Chemically Vapor-Deposited Silicon Carbide in Wet Oxygen," J. Am. Ceram. Soc. 77 [3] 730 (1994).
4. E.J. Opila and R.E. Hann, "Paralinear Oxidation of CVD SiC in Water Vapor," J. Am. Ceram. Soc., 80 [1] 197-205 (1997).
5. K.L. More, P.F. Tortorelli, M.K. Ferber, and J.R. Keiser, "Observations of Accelerated Silicon Carbide Recession by Oxidation at High Water-Vapor Pressures, J. Am. Ceram. Soc. 83 [1] 211-13 (2000).

6. Carruthers, W. D., Richerson, D. W., and Benn, K. W.,"3500-Hour Durability Testing of Commercial Ceramic Materials Interim Report", DOE/NASA/0027-80/1, NASA Report CR-159785, NASA Lewis Research Center, Cleveland, OH, 1980.

7. R.C. Robinson and J.L. Smialek, "SiC Recession Caused by SiO_2 Scale Volatility under Combustion Conditions: 1, Experimental Results and Empirical Model," J. Am. Ceram. Soc. 82 [7] 1817-25 (1999).

8. E.J. Opila, J.L. Smialek, R.C. Robinson, D.S. Fox, and N.S. Jacobson, "SiC Recession Caused by SiO_2 Scale Volatility under Combustion Conditions: 2, Thermodynamics and Gaseous Diffusion Model," J. Am. Ceram. Soc. 82 [7] 1826-34 (1999).

9. J.L. Smialek, R.C. Robinson, E.J. Opila, D.S. Fox, N.S. Jacobson, "SiC and Si_3N_4 Recession due to SiO_2 Scale Volatility under Combustor Conditions," Adv. Composite Mater., 8 [1] 33-45 (1999).

10. M.K. Ferber, H.T. Lin, V. Parthasarathy, and R.A. Wenglarz, "Degradation of Silicon Nitrides in High Pressure, Moisture Rich Environments," paper 2000-GT-0661 in Proceedings of IGTI Conference, Munich, ASME, May 8-11, 2000.

11. E.J. Opila, Paralinear Oxidation of SiC and Si_3N_4 in Combustion Environments, pp. 425-436 in Oxide Films, eds. K.R. Hebert, R.S. Lillard, and B. R. MacDougall, Electrochem. Soc., Pennington, NJ, 2000.

12. B.E. Deal and A.S. Grove, "General Relationship for the Thermal Oxidation of Silicon," J. Appl. Phys., 36 [12] 3770-78 (1965).

13. E.J. Opila and R.C. Robinson, "The Oxidation Rate of SiC in High Pressure Water Vapor Environments," pp. 398-406 in High Temp. Corr. Mat. Chem. 2, eds. M.J. McNallan, E.J. Opila, T. Maruyama, and T. Narita, Electrochem. Soc., Pennington, NJ, 2000.

14. E.J. Opila, "Variation of the Oxidation Rate of Silicon Carbide with Water-Vapor Pressure," J. Am. Ceram. Soc., 82 [3] 625-36 (1999).

15. R.H. Doremus, "Diffusion of Water in Silica Glass," J. Mater. Res. 10 [9] 2379-89 (1995).

16. A. Hashimoto, "The Effect of H_2O Gas on Volatilities of Planet-Forming Major Elements: 1. Experimental Determination of Thermodynamic Properties of Ca-, Al-, and Si-Hydroxide Gas Molecules and its Application to the Solar Nebula," Geochim. Cosmochim. Acta 56, 511-32 (1992).

17. D. Filsinger, A. Schulz, S. Wittig, H. Klemm, C. Taut, and G. Wötting, "Model Combustor to Assess the Oxidation Behavior of Ceramic Materials under Real Engine Conditions," paper 99-GT-349 in Proceedings of IGTI Conference, Indianapolis, IN, ASME, June 7-19, 1999.

18. Y. Etori, T. Hisamatsu, I. Yuri, U. Yasutomi, T. Machida, and K. Wada, "Oxidation Behavior of Ceramics for Gas Turbines in Combustion Gas Flow at 1500°C," paper 97-GT-355 in Proceedings of IGTI Conference, Orlando, FL, ASME, June 2-5, 1997.

19. E.J. Opila, "Influence of Alumina Reaction Tube Impurities on the Oxidation of Chemically-Vapor-Deposited Silicon Carbide," J. Am. Ceram. Soc. 78 [4] 1107-10 (1995).

20. Karren More, ORNL, private communication.

21. J.L. Smialek, J.A. Nesbitt, C.A. Barrett, and C.E. Lowell, "Cyclic Oxidation Testing and Modelling: a NASA Lewis Perspective," pp. 148-168 in Cyclic Oxidation of High Temperature Materials, European Federation of Corrosion Publications, number 27, IOM Communications, London, Great Britain, 1999.

Table 1.
Experimentally determined pressure, temperature, and gas velocity dependence of oxidation and volatilization rate constants for SiC in water vapor.

n, $P(H_2O)^n$	T dependence (kJ/mol)	m, v^m	Comments, reference
Parabolic oxidation rate, k_p			
0.67±0.19 0.85±0.05	28 to 156	n/a	not corrected for O_2 contribution, (4)
1.0	68	n/a	silicon, (12)
0.91±0.10	--	n/a	(13)
--	35±147	n/a	(4)
Linear volatilization rate, k_l			
1.50±0.13	108±7	0.50±0.16	(7)
--	56.7±1.7	--	(16)
--	3±75	--	(4)

Table 2.
Summary of relationships describing steady state paralinear oxidation/volatilization.

	Limiting oxide thickness	Time to steady state	Steady state recession rate
As a function of rate constants	$x_L = k_p / 2k_l$	$t_L = k_p / 2k_l^2$	$\dot{y}_L \propto k_l$
As a function of variables	$x_L \propto (Pv)^{-1/2}$	$t_L \propto (P^2 v)^{-1}$	$\dot{y}_L \propto P^{3/2}\, v^{1/2}$
Temperature dependence	$x_L \propto \exp\left(\frac{\Delta H_{vol} - \Delta H_{ox}}{RT}\right)$	$t_L \propto \exp\left(\frac{2\Delta H_{vol} - \Delta H_{ox}}{RT}\right)$	$\dot{y}_L \propto \exp\left(\frac{-\Delta H_{vol}}{RT}\right)$

Table 3.
Summary of test conditions for SiC and Si_3N_4 exposed in combustion environments.

Exposure, reference	material	P, atm	$P(H_2O)$, atm	v, m/s	T, °C	Approximate time (h)
A. furnace 1 (3)	SiC	1	0.1	0.0044	1200-1400	100
B. furnace 2 (4)	SiC	1	0.5	0.044	1200-1400	100
C. high pressure furnace (5)	SiC Si_3N_4	10	1.5	$5x10^{-4}$	1200	500
D. mach 0.3 burner rig (6)	SiC	1	0.1	100	1200-1400	3500
E. high pressure burner rig (7)	SiC	5.7	0.7	20	1200-1450	100
F. turbine (10)	Si_3N_4	8.7	0.87	573	1066-1260	815

Table 4.
A comparison of measured oxidation and volatilization rate constants with rate constants calculated from Equations 10 and 15.

	k_p, μ^2 SiO_2/h		k_l, μ SiO_2/h	
	calculated	measured	calculated	measured
A. laboratory furnace 1 (3)	0.044	0.062	$2.4x10^{-4}$	NA
B. laboratory furnace 2 (4)	0.22	0.40	$1.9x10^{-2}$	$1.3x10^{-2}$
C. high pressure furnace (5)	0.66	NA*	$5.7x10^{-3}$	NA*
D. mach 0.3 burner rig (unpublished work)	0.044	NA	$3.6x10^{-2}$	$2.0x10^{-2}$
E. high pressure burner rig (13,7)†	0.31	0.31	$3.3x10^{-1}$	$3.3x10^{-1}$
F. turbine (10)	0.39	NA	2.2	0.2-1.5

*Under these conditions a non-protective scale is formed on SiC, paralinear oxidation/volatilization does not occur and the rate constants are not physically meaningful in the context of the paralinear mechanism.

†Calculated and measured values are identical for this case since Equations 10 and 15 are based on these measurements.

Table 5.
Summary of calculated and observed oxide thickness for SiC and Si_3N_4 exposed in combustion environments.

Exposure, reference	x_L, μ	t_L, h	x measured, μ	t measured, h	$t>t_L$
A. furnace 1 (3)	91	$4x10^5$	1.9-2.8	100	
B. furnace 2 (4)	6	300	2.5-4.5	100	
C. high pressure furnace* (5)	58	$1x10^4$	25-30 50-60	100 500	
D. mach 0.3 burner rig (unpublished work)	0.6	17	2-7	200	✓
E. high pressure burner rig (7)	0.6	3	2-6	100	✓
F. turbine (10)	0.1	2 min.	none detected	815	✓

*Paralinear behavior not observed under these conditions. x_L and t_L would be meaningful if a dense scale was formed.

Table 6.
Steady state recession rates calculated from Equation 21 for SiC at 1316°C under conditions in Table 3 assuming paralinear oxidation/volatilization.

	$\dot{y}$, μ SiC/h
A. Furnace 1	$2x10^{-4}$
B. Furnace 2	$2x10^{-2}$
C. High pressure furnace	$6x10^{-3}$
D. Mach 0.3 burner rig	$4x10^{-2}$
E. High pressure burner rig	$3x10^{-1}$
F. turbine	2

Table 7.
Limits for paralinear oxidation/volatilization.

limit	velocity	pressure	controlling recession mechanism
1. negligible volatilization/ recession	low	low	parabolic oxidation rate
2. long time constant	low	low	parabolic oxidation rate
3a. non-protective scale	low	high	rate of oxidant transport through porous scale
3b. thick spalling scale	low	high	parabolic oxidation rate, spallation rate?
4. thin or missing scale	high	high	linear oxide growth rate? active hydroxide formation?

LIST OF FIGURES

Figure 1. Dimensional change for SiC due to paralinear oxidation and volatilization. Oxide thickness and SiC recession curves calculated for k_p=0.25 μ^2/h and k_l=0.21 μ/h..

Figure 2. Determination of the time constant for achieving steady state oxide thickness. The solid curve represents paralinear oxide growth. The dotted lines represent oxide thickness for parabolic kinetics and the steady state oxide thickness. Oxide thickness and time are normalized by x_L and $t_{c,o}$, respectively.

Figure 3. Determination of the time constant for achieving the steady state recession rate. The solid curve represents paralinear recession. The dotted lines represent recession for parabolic kinetics and the steady state recession. Recession depth and time are normalized by $y_n=k_p'/k_l'$ and $t_{c,r}$, respectively.

Figure 4. Limiting oxide thickness map calculated in terms of the oxidation and volatilization rate constants for SiC at 1316°C.

Figure 5. Steady state time constant map calculated in terms of the oxidation and volatilization rate constants for SiC at 1316°C.

Figure 6. Limiting oxide thickness map calculated in terms of the total pressure and gas velocity for SiC at 1316°C in a hydrocarbon combustion environment.

Figure 7. Steady state time constant map calculated in terms of the total pressure and gas velocity for SiC at 1316°C in a hydrocarbon combustion environment.

Figure 8. Steady state recession rate map calculated in terms of the total pressure and gas velocity for SiC at 1316°C in a hydrocarbon combustion environment.

Figure 9. Representative oxide cross-sections formed on silica-formers for each of the case studies. A) laboratory furnace 1: CVD SiC, 1300°C, 1 atm, 10% H_2O/90% O_2, 0.4 cm/s, 113h. B) laboratory furnace 2: CVD SiC, 1300°C, 1 atm, 50% H_2O/50% O_2, 4.4 cm/s, 100h. C) high pressure furnace: CVD SiC (left), AS800 Si_3N_4 (right), 1200°C, 10 atm, 15% H_2O, 0.05 cm/s, 500h. D) mach 0.3 burner rig: sintered SiC, 1300°C, 1 atm, 10% H_2O, 100 m/s, 200h. E) high pressure burner rig: CVD SiC, 1316 °C, 5.5 atm, 10% H_2O, 20 m/s, 98h. F) turbine: AS800 Si_3N_4, 1066-1260°C, 8.9 atm, 10% H_2O, 162-573 m/s, 815h.

Figure 10. Limits for the paralinear oxidation and volatilization model mapped in terms of total pressure and gas velocity for SiC at 1316°C in a hydrocarbon combustion environment. The dots represent the case studies referred to in Table 3.

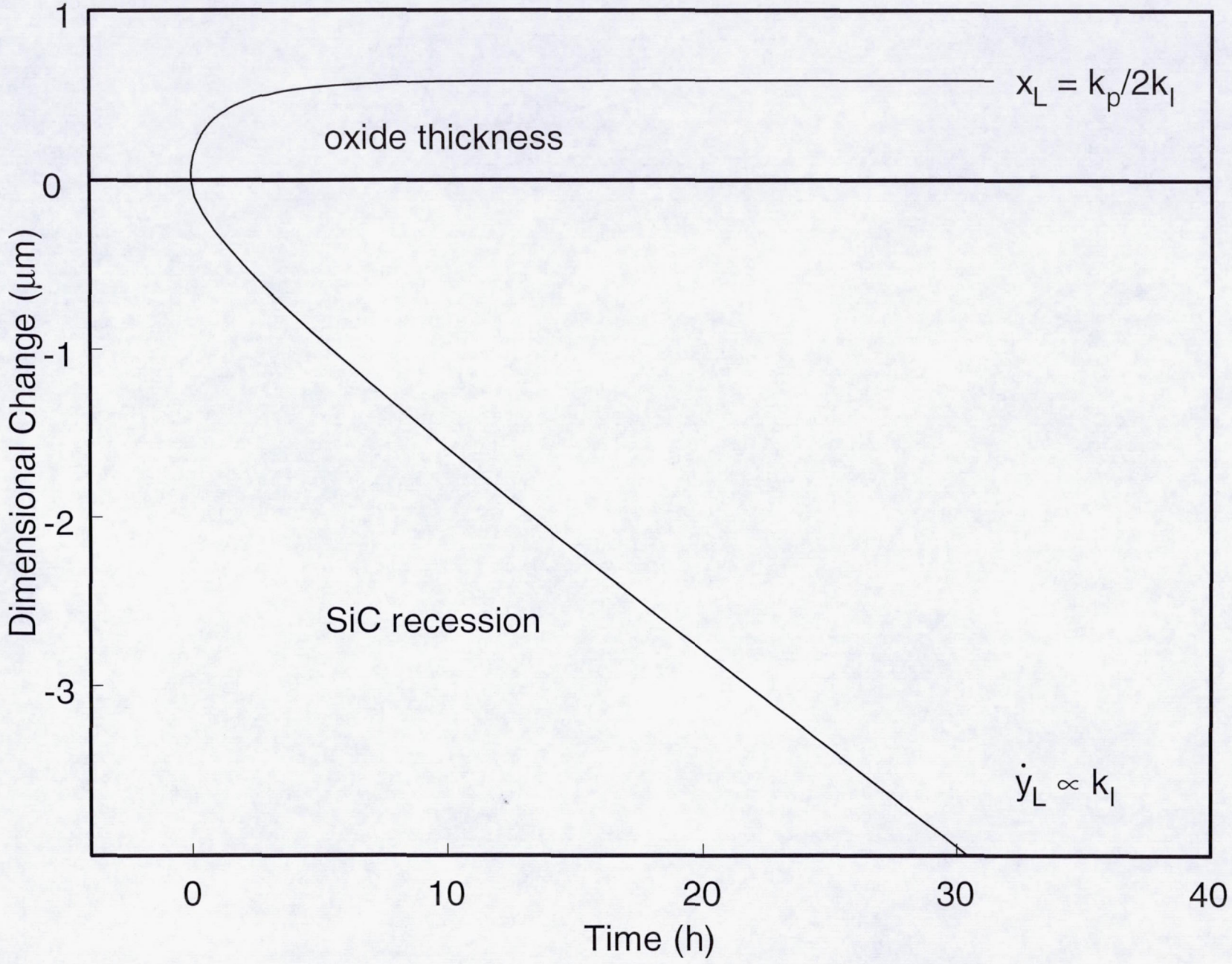
1
0
-1
-2
-3
Dimensional Change (μm)
oxide thickness
$x_L = k_p/2k_l$
SiC recession
$\dot{y}_L \propto k_l$
0
10
20
30
40
Time (h)

Fig. 1

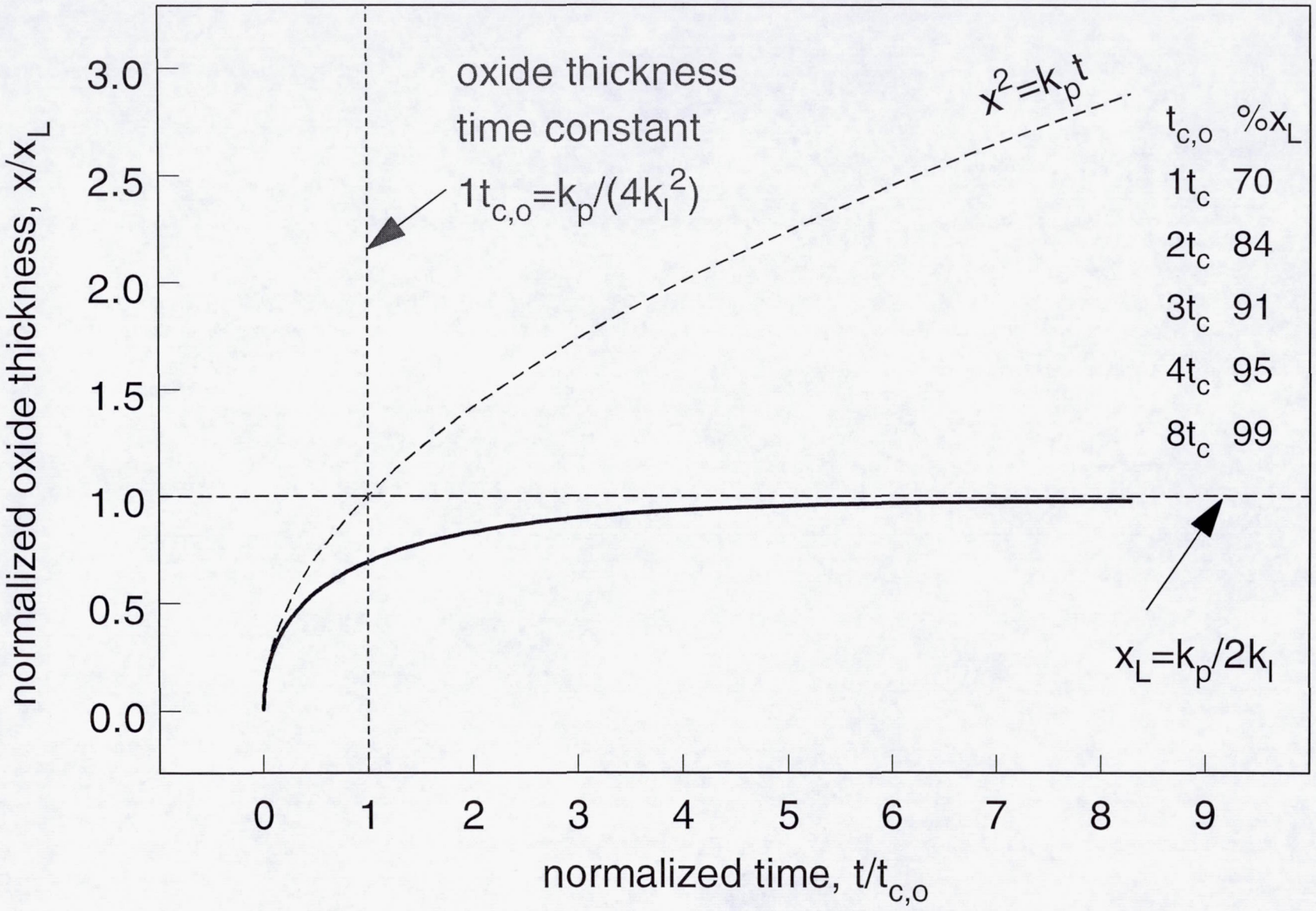
normalized oxide thickness, x/x_L
3.0
2.5
2.0
1.5
1.0
0.5
0.0
oxide thickness
time constant
$1t_{c,o}=k_p/(4k_l^2)$
$x^2=k_p t$
$t_{c,o}$ $\%x_L$
$1t_c$ 70
$2t_c$ 84
$3t_c$ 91
$4t_c$ 95
$8t_c$ 99
$x_L=k_p/2k_l$
0 1 2 3 4 5 6 7 8 9
normalized time, $t/t_{c,o}$

Fig. 2

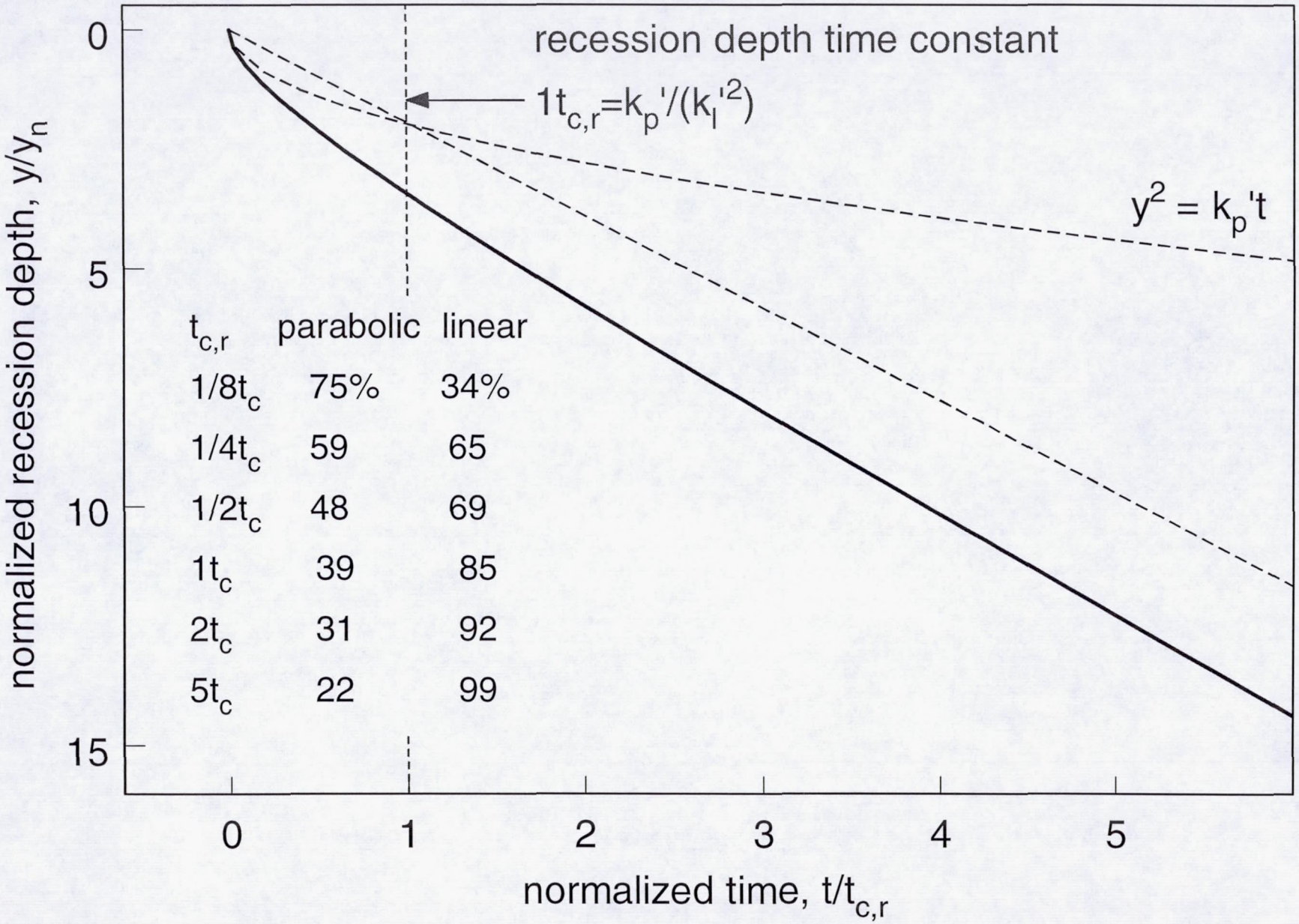
recession depth time constant
$1t_{c,r}=k_p'/(k_l'^2)$
$y^2 = k_p't$
$t_{c,r}$ parabolic linear
$1/8t_c$ 75% 34%
$1/4t_c$ 59 65
$1/2t_c$ 48 69
$1t_c$ 39 85
$2t_c$ 31 92
$5t_c$ 22 99
normalized recession depth, y/y_n
normalized time, $t/t_{c,r}$
0
5
10
15
0
1
2
3
4
5

Fig. 3

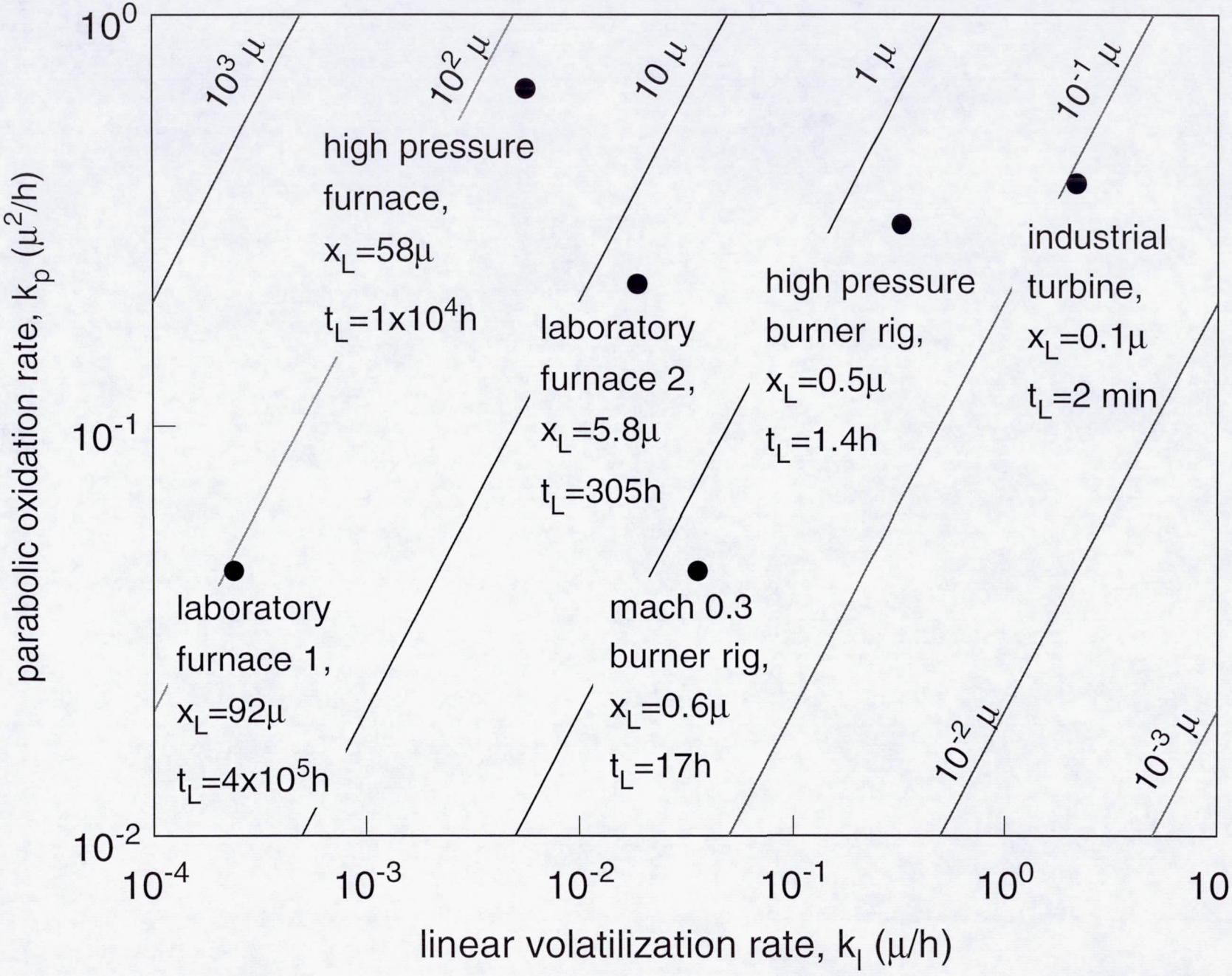
10^0
10^{-1}
10^{-2}
10^{-4}
10^{-3}
10^{-2}
10^{-1}
10^0
10^1
parabolic oxidation rate, k_p (μ^2/h)
linear volatilization rate, k_l (μ/h)
$10^3\,\mu$
$10^2\,\mu$
$10\,\mu$
$1\,\mu$
$10^{-1}\,\mu$
$10^{-2}\,\mu$
$10^{-3}\,\mu$
high pressure furnace, x_L=58μ t_L=1x10^{4}h
laboratory furnace 2, x_L=5.8μ t_L=305h
high pressure burner rig, x_L=0.5μ t_L=1.4h
industrial turbine, x_L=0.1μ t_L=2 min
laboratory furnace 1, x_L=92μ t_L=4x10^{5}h
mach 0.3 burner rig, x_L=0.6μ t_L=17h

Fig. 4

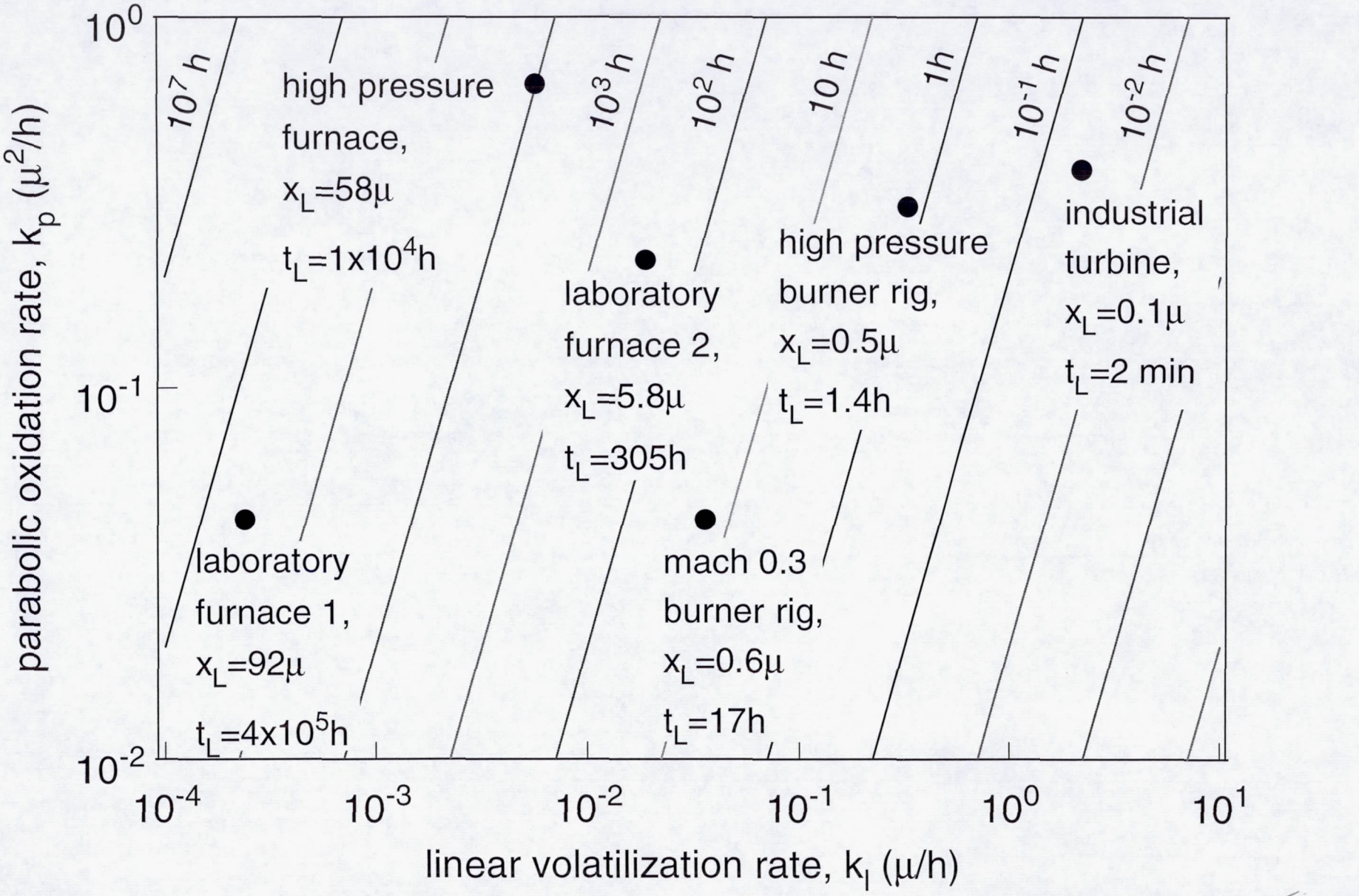
parabolic oxidation rate, k_p (μ^2/h)
linear volatilization rate, k_l (μ/h)
10^0
10^{-1}
10^{-2}
10^{-4}
10^{-3}
10^{-2}
10^{-1}
10^0
10^1
10^7 h
10^3 h
10^2 h
10 h
1h
10^{-1} h
10^{-2} h
high pressure furnace, x_L=58μ t_L=1x10^{4}h
laboratory furnace 2, x_L=5.8μ t_L=305h
high pressure burner rig, x_L=0.5μ t_L=1.4h
industrial turbine, x_L=0.1μ t_L=2 min
laboratory furnace 1, x_L=92μ t_L=4x10^{5}h
mach 0.3 burner rig, x_L=0.6μ t_L=17h

Fig. 5

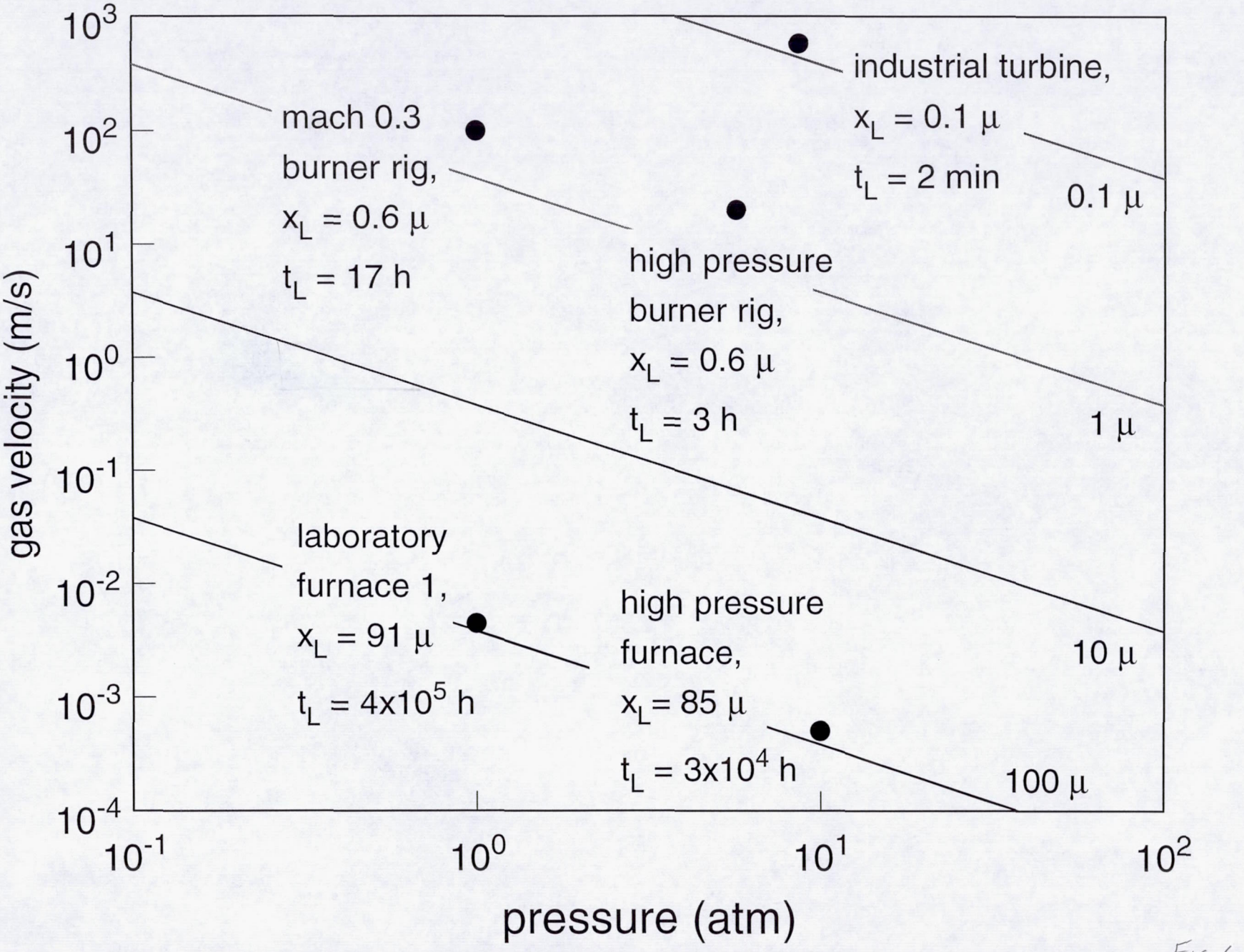
gas velocity (m/s)
10^3
10^2
10^1
10^0
10^{-1}
10^{-2}
10^{-3}
10^{-4}
10^{-1}
10^0
10^1
10^2
pressure (atm)
industrial turbine,
x_L = 0.1 μ
t_L = 2 min
0.1 μ
mach 0.3
burner rig,
x_L = 0.6 μ
t_L = 17 h
high pressure
burner rig,
x_L = 0.6 μ
t_L = 3 h
1 μ
laboratory
furnace 1,
x_L = 91 μ
t_L = $4x10^5$ h
high pressure
furnace,
x_L = 85 μ
t_L = $3x10^4$ h
10 μ
100 μ

Fig. 6

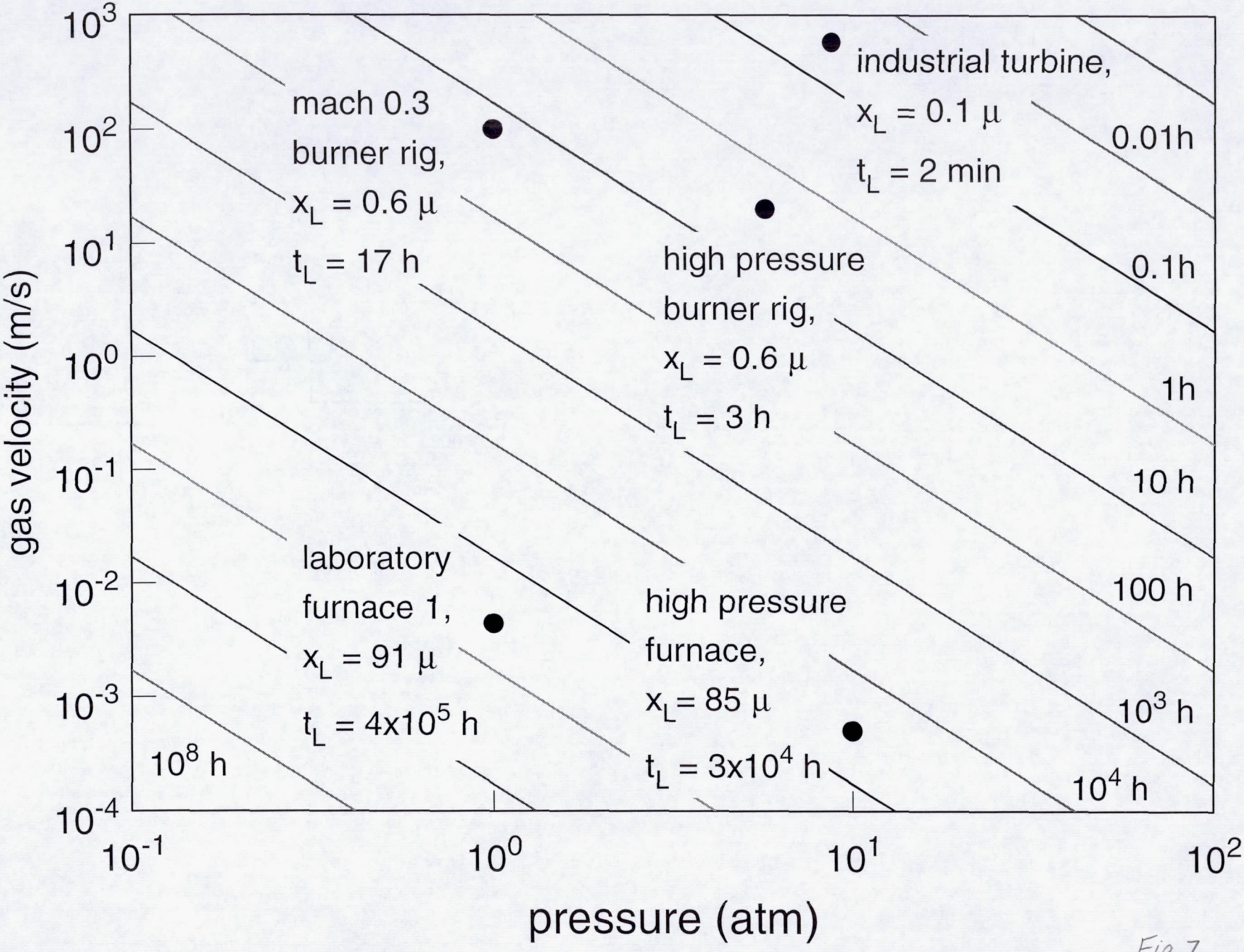
gas velocity (m/s)
10^3
10^2
10^1
10^0
10^{-1}
10^{-2}
10^{-3}
10^{-4}
10^{-1}
10^0
10^1
10^2
pressure (atm)
mach 0.3
burner rig,
x_L = 0.6 μ
t_L = 17 h
industrial turbine,
x_L = 0.1 μ
t_L = 2 min
high pressure
burner rig,
x_L = 0.6 μ
t_L = 3 h
laboratory
furnace 1,
x_L = 91 μ
t_L = $4x10^5$ h
high pressure
furnace,
x_L = 85 μ
t_L = $3x10^4$ h
0.01h
0.1h
1h
10 h
100 h
10^3 h
10^4 h
10^8 h

Fig. 7

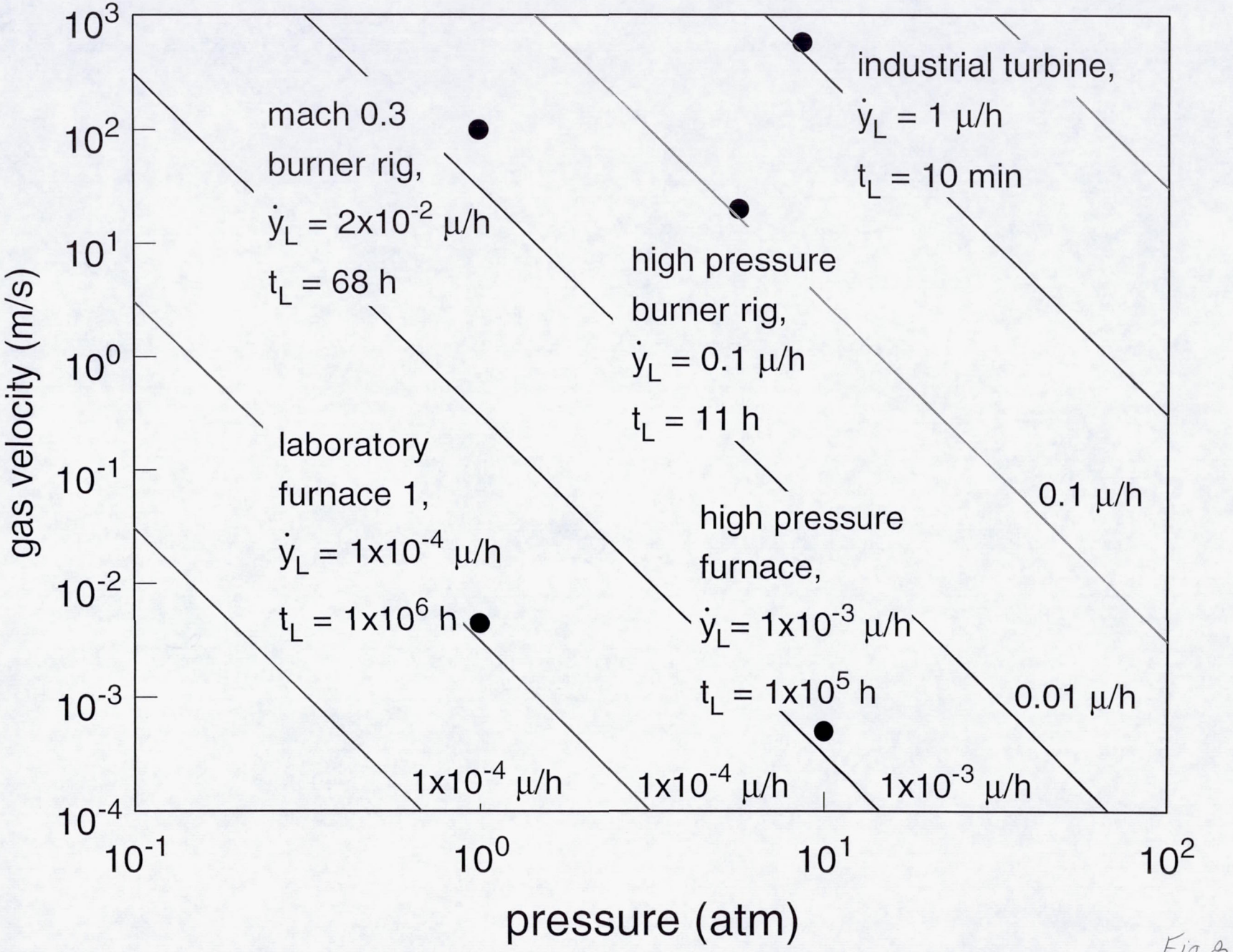
gas velocity (m/s)
10^3
10^2
10^1
10^0
10^{-1}
10^{-2}
10^{-3}
10^{-4}
10^{-1}
10^0
10^1
10^2
pressure (atm)
mach 0.3
burner rig,
$\dot{y}_L = 2x10^{-2}$ μ/h
t_L = 68 h
industrial turbine,
$\dot{y}_L$ = 1 μ/h
t_L = 10 min
high pressure
burner rig,
$\dot{y}_L$ = 0.1 μ/h
t_L = 11 h
laboratory
furnace 1,
$\dot{y}_L = 1x10^{-4}$ μ/h
$t_L = 1x10^6$ h
high pressure
furnace,
$\dot{y}_L = 1x10^{-3}$ μ/h
$t_L = 1x10^5$ h
0.1 μ/h
0.01 μ/h
$1x10^{-4}$ μ/h
$1x10^{-4}$ μ/h
$1x10^{-3}$ μ/h

Fig. 8

Fig. 9a

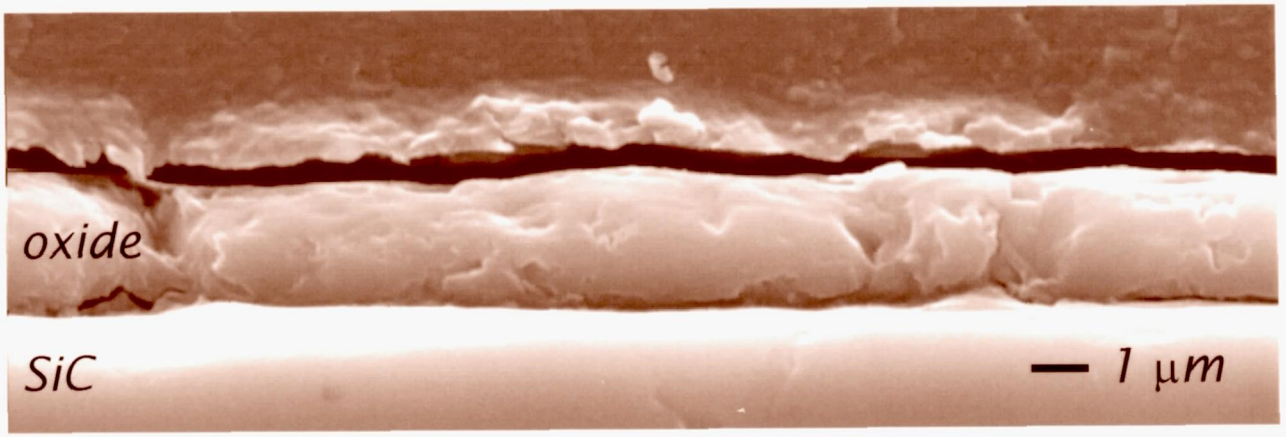

CVD SiC, 1300°C, 1 atm, 10% H_2O/90% O_2, 0.4 cm/s, 113h

Fig. 9b

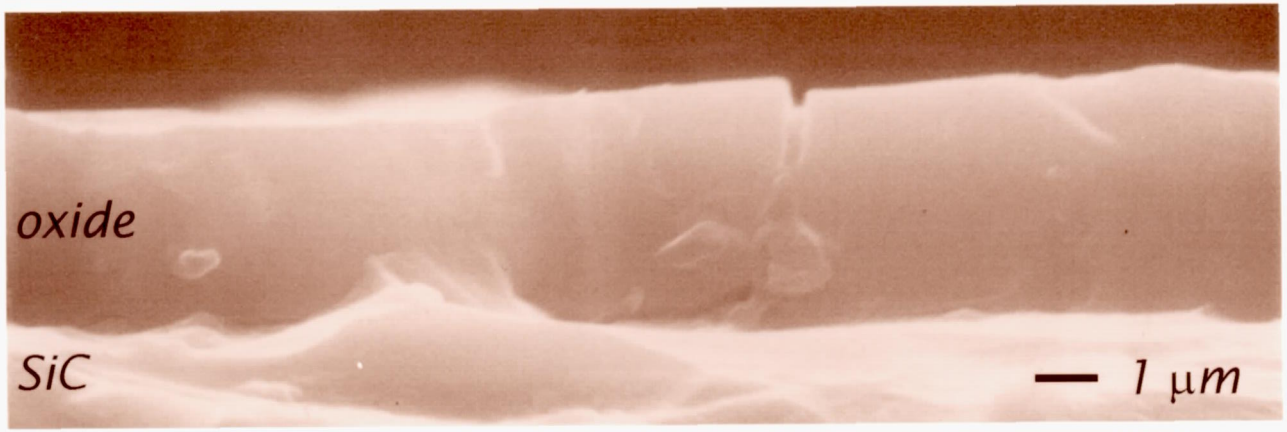

CVD SiC, 1300°C, 1 atm, 50% H_2O/50% O_2, 4.4 cm/s, 100h

Fig. 9c

1200°C, 10 atm, 15% H_2O, 0.05 cm/s, 500h

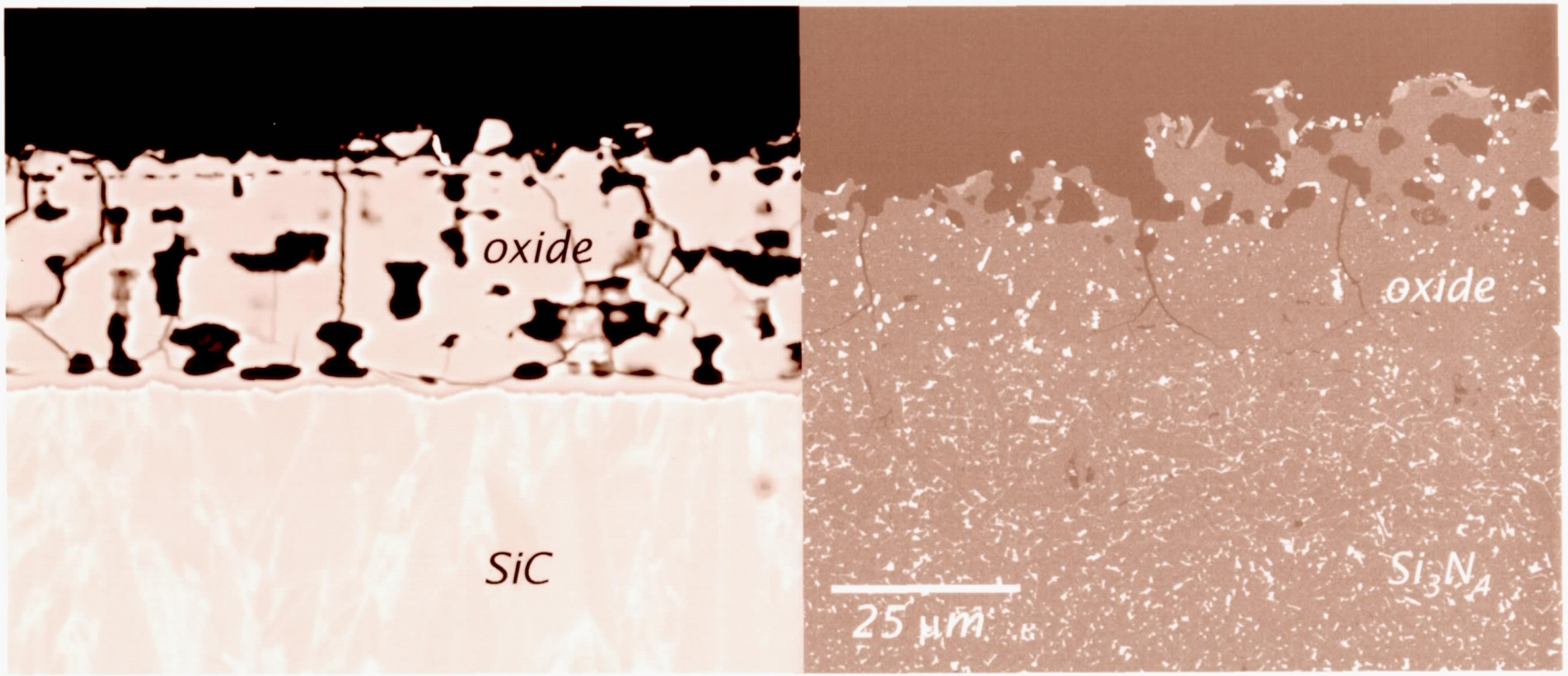

CVD SiC

AS800 Si_3N_4

Micrographs courtesy Karren More, ORNL

Fig. 9d Sintered SiC, 1300°C, 1 atm, 10% H_2O, 100 m/s, 200h

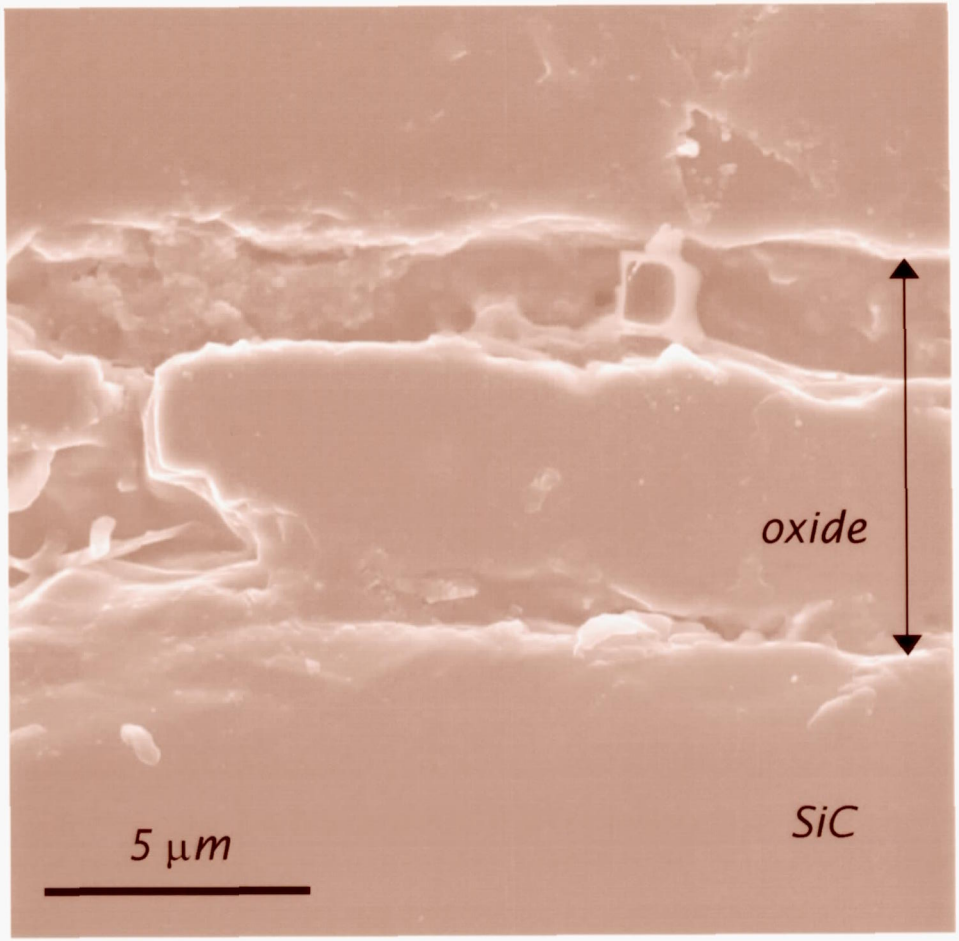

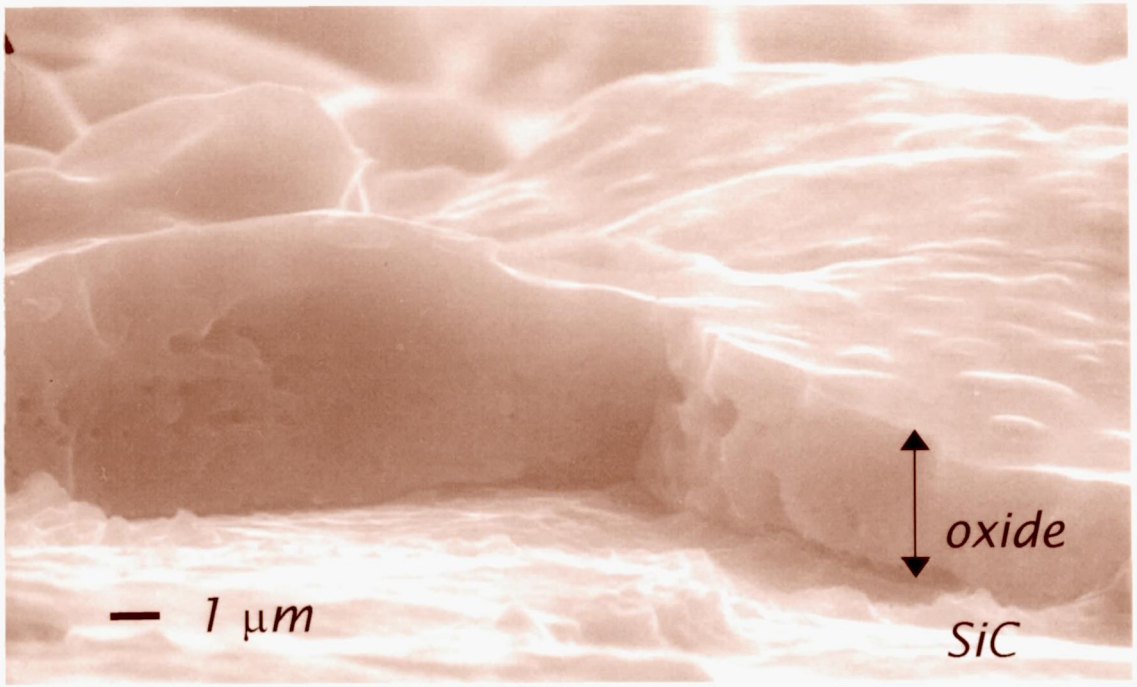

Fig. 9e CVD SiC, 1316 °C, 5.5 atm, 20 m/sec, 98h

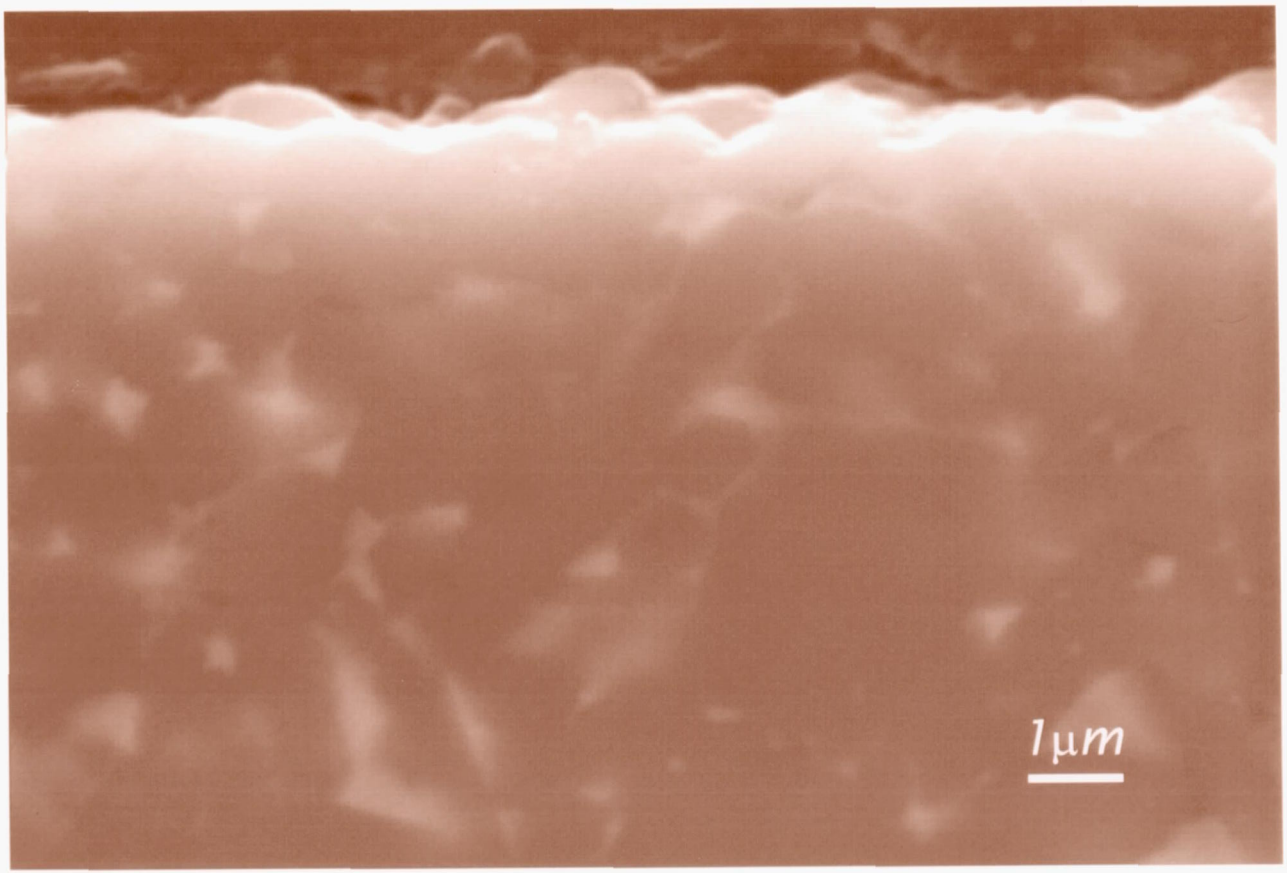

Fig. 9f AS800 Si_3N_4, 1066-1260°C, 8.9 atm, 10% H_2O, 162-573 m/s, 815h

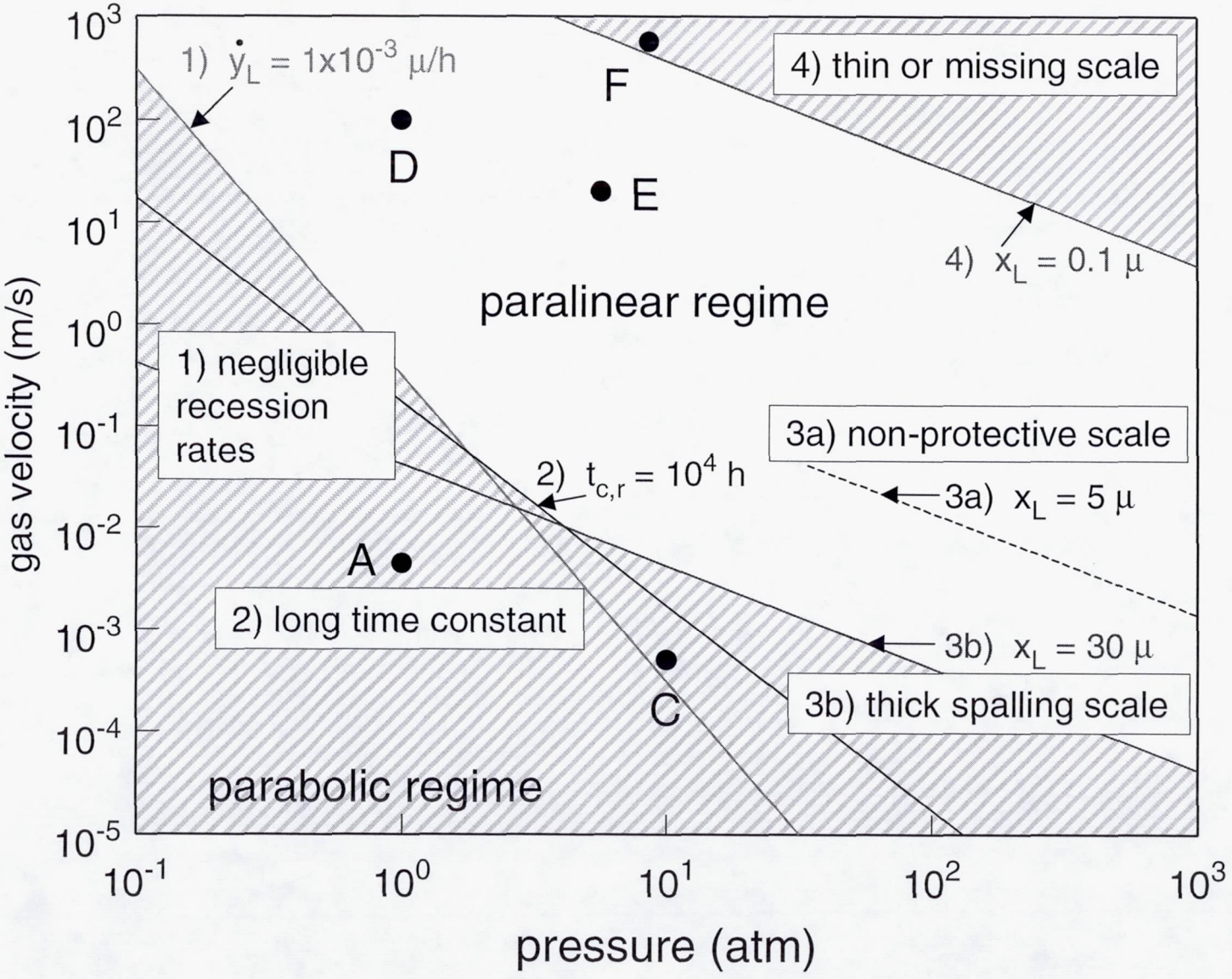
gas velocity (m/s)
pressure (atm)
10^3
10^2
10^1
10^0
10^{-1}
10^{-2}
10^{-3}
10^{-4}
10^{-5}
10^{-1}
10^0
10^1
10^2
10^3
1) $\dot{y}_L$ = 1x10^{-3} μ/h
4) thin or missing scale
F
D
E
4) x_L = 0.1 μ
paralinear regime
1) negligible recession rates
3a) non-protective scale
2) $t_{c,r}$ = 10^4 h
3a) x_L = 5 μ
A
2) long time constant
3b) x_L = 30 μ
C
3b) thick spalling scale
parabolic regime

Fig. 10